(2)

AD _____

Contract No: DAMD17-88-C-8125

Title: Spectroscopy of Burn Wounds

Principal Investigator: Martin A. Afromowitz, Ph.D.

PI Address:
University of Washington
Department of Electrical Engineering
FT-10
Seattle, WA 98195

Co-Principal Investigator: James B. Callis, Ph.D.

Co-PI Address:
University of Washington
Department of Chemistry
BG-10
Seattle, WA 98195

Report Date: April 1, 1990

Type of Report: Annual Report
July 15, 1988 — July 14, 1989

Prepared for: U. S. Army Medical Research
& Development Command
Fort Detrick
Frederick, MD 21701-5012

SECURITY CLASSIFICATION OF THIS PAGE

REPORT DOCUMENTATION PAGE

Form Approved OMB No. 0704-0188

1a. REPORT SECURITY CLASSIFICATION Unclassified	1b. RESTRICTIVE MARKINGS
2a. SECURITY CLASSIFICATION AUTHORITY	3 DISTRIBUTION/AVAILABILITY OF REPORT Approved for public release; distribution unlimited
2b. DECLASSIFICATION/DOWNGRADING SCHEDULE	
4. PERFORMING ORGANIZATION REPORT NUMBER(S)	5. MONITORING ORGANIZATION REPORT NUMBER(S)
6a. NAME OF PERFORMING ORGANIZATION University of Washington 6b. OFFICE SYMBOL (If applicable)	7a. NAME OF MONITORING ORGANIZATION
6c. ADDRESS (City, State, and ZIP Code) Department of Electrical Engineering FT-10 Seattle, WA 98195	7b. ADDRESS (City, State, and ZIP Code)
8a. NAME OF FUNDING/SPONSORING ORGANIZATION U.S. Army Medical Research & Development Command 8b. OFFICE SYMBOL (If applicable)	9. PROCUREMENT INSTRUMENT IDENTIFICATION NUMBER Contract No. DAMD17-88-C-8125
8c. ADDRESS (City, State, and ZIP Code) Fort Detrick Frederick, Maryland 21701-5012	10. SOURCE OF FUNDING NUMBERS PROGRAM ELEMENT NO. 63002A; PROJECT NO. 3M2 63002D840; TASK NO. DA; WORK UNIT ACCESSION NO. 001

11. TITLE (Include Security Classification)

SPECTROSCOPY OF BURN WOUNDS

12. PERSONAL AUTHOR(S)

Martin A. Afromowitz, Ph.D., and James B. Callis, Ph.D.

13a. TYPE OF REPORT	13b. TIME COVERED	14. DATE OF REPORT (Year, Month, Day)	15. PAGE COUNT
Annual Report	FROM 7/15/88 TO 7/14/89	1990 April 1	50

16. SUPPLEMENTARY NOTATION

17. COSATI CODES			18. SUBJECT TERMS (Continue on reverse if necessary and identify by block number)
FIELD	GROUP	SUB-GROUP	
06	05		RA II; Volunteers; Burn Wounds; Burn Depths; Diagnosis; Instrument
06	12		

19. ABSTRACT (Continue on reverse if necessary and identify by block number)

This research seeks to develop non-invasive techniques for evaluating burn depth based upon non-contacting visible and near- infrared spectroscopic measurement of the wounds. In previous years, we demonstrated that features of the optical reflection spectra of burn wounds can be correlated with the depth of burn. An imaging system was built which determined, with accuracy equal to or better than that of a skilled burn surgeon, the probability that burn sites would heal within three weeks from date of injury. Our goal for the current project is to investigate the optical reflectance properties of burns, utilizing the techniques of multivariate analysis, in order to improve the reliability of this instrument and to develop methods which will permit detailed monitoring of the healing process.

A commercial spectrophotometer, LT Quantum 1200, was modified to make optical reflection measurements from the surface of the wounds of burn patients without contacting them.

20. DISTRIBUTION/AVAILABILITY OF ABSTRACT ☐ UNCLASSIFIED/UNLIMITED ☐ SAME AS RPT ☐ DTIC USERS	21 ABSTRACT SECURITY CLASSIFICATION Unclassified
22a. NAME OF RESPONSIBLE INDIVIDUAL Virginia M. Miller	22b TELEPHONE (Include Area Code) (301) 663-7325 22c. OFFICE SYMBOL SGRD-RMI-S

DD Form 1473, JUN 86 Previous editions are obsolete. SECURITY CLASSIFICATION OF THIS PAGE

19. ABSTRACT (Continued)

Spectra can now be measured in the near-infrared region (900-1800 nm) and we hope to be able to make similar measurements in the visible region (450-900 nm) in the near future. This instrument has been used to acquire a library of reference spectra, both *in vitro* and *in vivo*.

A number of experiments have been performed in order to understand the major components of the reflectance spectra of human skin *in vivo*. Nearly all of the spectral features can now be explained in terms of the constituent biochemical composition of live skin. Two major components of skin tissue, hemoglobins and water, have been studied in some detail, using models approximating changes that are expected in burn wounds. The variation in the oxygenation of hemoglobin during reduced circulation was successfully observed non-invasively and an extensive study of hydrogen bonding in water was begun.

In order to understand the nature of hydrogen bonds in pure water and their spectroscopic manifestations in NIR spectra, precision measurements of water overtone peaks in the range 680 – 1235 nm were made over a wide range of temperatures. With the aid of contemporary mathematical tools, the mixture model of water was verified and found to require three components. This model can predict the temperature of unknown spectra within 0.2° C.

FOREWORD

For the protection of human subjects, the investigator(s) have adhered to policies of applicable Federal Law 45CFR56.

Citations of commercial organizations and trade names in this report do not constitute an official Department of the Army endorsement or approval of the products or services of these organizations.

RESEARCH RESULTS

I. Instrument Selection, Installation and Testing.

A. Selection of the LT Quantum 1200 Spectrophotometer.

Our first task was to select and purchase a Visible/Near-infrared spectrophotometer suitable for non-contacting spectroscopy of biological tissues. Manufactures of commercial near-infrared (NIR) spectrophotometers were surveyed. Three vendors, Pacific Scientific, L.T. Industries (LT), and Technicon produced instruments which could be modified to obtain spectra from human skin *in vivo*. Only the LT Quantum 1200 proved suitable for obtaining spectra of open wounds. The following are features that were considered crucial to project success.

1. Fiber Optic Reflectance Probe. The LT instrument uses a special probe to collect light reflected from the burn wound. It does not require the skin to be contacted. Other vendors' probes based on fiber optics must contact the sample in order to collect enough scattered light. For open wounds, this is highly impractical. In order to collect light at a distance a probe must have either a collecting sphere or a reflectance detector positioned near the sample surface. The LT instrument employs the later configuration and the detector head can be remotely mounted on a camera tripod.

2. Wavelength Range. The LT instrument has the potential to scan 450-1800 nm with a single filter change. This switch would take two seconds. In contrast most NIR spectrometers require two sets of optical components in order to scan both the visible range (400-700 nm) and the NIR range (700-1800 nm). Switching and realigning the optics can take up to 3 hours. It is not possible to ask patients to wait that long.

3. Scan Rate. The LT instrument can scan at 300 spectra per minute, compared to 150 and 1 per minute for the Pacific Scientific

and Technicon instruments respectively. This is important for exposed burns which dry out and become painful if they are left open for more than a few minutes.

4. Size. The LT is the only instrument small enough to be moved around the hospital, from room to room everyday, and at the same time, have a spectral resolution of as narrow as 1 nm.

B. Validation of Performance.

1. Baseline Noise. The baseline signal to noise ratio of the spectrometer is still too low for good spectra acquisition, particularly in the visible region. The baseline noise in the NIR region is 170 micro absorbance units (μ a.u.) at 0.0 optical density (o.d.) and 1400 μ a.u. at 1.0 o.d. (Figure 1a-b). The noise in the visible is 540 μ a.u. and 4400 μ a.u. Noise levels less than 25 μ a.u. and 50 μ a.u. are desirable. We suspect that the optical coupling between the instrument and the modified fiber optic probe is causing loss of signal. We are investigating alternative coupling methods and have ordered a silicon detector which will be more sensitive to visible light.

2. Scan speed. The average scan speed is 4.9 spectra/sec. When 100 scans are averaged the time required to scan 450-1800 nm, including filter change, would be 43 seconds.

3. Wavelength calibration. The wavelength scale was calibrated with a National Bureau of Standards' NIR wavelength standard (Figure 2) and a didymium filter (Figure 3).

II. Establishment of a Library of Standard Spectra and Peak Assignments.

Reflection spectra of skin tissues are dominated in the visible region by electronic transitions of hemes, cytochromes and melanin. The absorption bands of these molecules are very broad and quite intense. Maximum molar absorptivities of hemes are $10\text{-}20 \times 10^3$ (L

mol^{-1} cm^{-1}) in the 450-650 nm region. NIR absorbances, in contrast, are largely due to overtones and combinations of vibrational transitions. They also are relatively more narrow but are very weak. Here the molar absorptivities are in the range 10^{-3}-10^{-1}. Due to the fact that water constitutes 70-90% of tissue, its spectrum dominates. Nevertheless, other species (fat, muscle, connective tissue) have characteristic absorbances in the NIR which can be observed against a water background.

The broad bands in both regions tend to overlap one another, which makes spectral interpretation somewhat difficult. Second derivative spectra are often used to increase resolution and render the data more interpretable. An example of the effect of a second derivative transformation on an artificial gaussian peak is shown in Figure 4a,b. Another use of derivatives is to remove baseline slopes and offsets (Figure 4c,d). These are caused by variations in diffuse and specular reflectance at the surface and scattering within the tissues, factors which are irrelevant to most of the studies discussed here. Therefore, most spectra will be presented as derivative spectra, except where important scattering effects are discussed.

Standard NIR reference spectra were obtained from water, mineral oil, fat, muscle tissue (pork, beef, chicken, and lamb), tendons, skin, and collagen. Spectra were also obtained from normal and scarred human skin *in vivo*. Peak assignments were made from Colthup type charts and other data found in the book edited by Phil Williams and Karl Norris (1) and are listed in Table I. Distilled water (Figure 5), mineral oil (Figure 6), and extracted collagen (Figure 7) from Sigma Co. are representative of water, hydrocarbon (fat), and protein (muscle, connective tissue, skin), the three main components of tissues. The transitions for water are due to combination bands involving H-OH stretching and bending, while for hydrocarbons they arise from overtones of the $-CH_3$ and $-CH_2$ stretching and combinations of stretch and bend motions. Proteins exhibit $-CH_2$, $-CH_3$, -OH, and -NH bands. Peak assignments were

verified by studying the corresponding individual tissues: muscle, fat, tendon, and skin. Spectra of fat (Figure 8) contain primarily hydrocarbon absorbances plus a very small amount of water. Muscle spectra (Figure 9) contain absorbances due to water, fat, and protein. The hydrocarbon bands from fat vary in intensity with the leanness of the muscle tissue (Figure 10). Note particularly the ratio of the -OH combination band to the $-CH_3$ stretch. Beef, being the most fatty, shows the lowest ratio. Bovine tendon (Figure 11) shows primarily water and collagen, though in this spectrum the high absorbance of water obscures the weaker collagen peaks in the 1400-1800 nm range. Rat skin (Figure 12) also shows water and collagen plus large peaks from a subcutaneous layer of fat. Note that the hydrocarbon bands of collagen are significantly shifted due to the amino acid proline and are clearly distinguishable from those of fat.

It is important to realize that the reflectance spectra of these tissues and of human skin *in vivo* (Figure 13) are not simple sums of the spectra of their constituents. Rather, the constituent spectra are distorted according to the structure of the tissues in which they are embedded. Despite the high degree of non-linearity, it is possible to obtain useful information about each of the layers of tissue.

For non-scattering samples, transmission spectra of individual components follow the relationship:

$$A_j = b * a_j * c \qquad (1)$$

A_j = absorbance measured by instrument at the j^{th} wavelength
a_j = absorptivity at the j^{th} wavelength, a characteristic constant of the compound
b = path length of light through sample = thickness of sample
c = concentration

For mixtures, the spectral contribution of each component is often

found to be proportional to its concentration.

$$A_j = b * {}_i\Sigma\ (a_{ij} * c_i) \qquad (2)$$

a_{ij} = absorptivity of the i^{th} component at the j^{th} wavelength
c_i = concentration of the i^{th} component in the sample

In reflectance spectroscopy, the path length is no longer defined by the dimensions of the sample. Instead, light is scattered randomly in the sample. To a first approximation the path length can be considered to be the average distance light travels in the sample before returning to the spectrometer, and it is wavelength dependent. Now equation 2 becomes

$$A_j = b_j * {}_i\Sigma\ (a_{ij} * c_i) \qquad (3)$$

b_j = average distance traveled by light of wavelength j

In a multilayered sample like skin, the path length is also a function of the composition and thickness of the layers. Constituent concentrations vary as well.

$$A_j = {}_k\Sigma\ (\ b_{jk} * {}_i\Sigma\ (a_{ij} * c_{ik})\ ) \qquad (4)$$

b_{jk} = path length in k^{th} layer
c_{ik} = concentration of i^{th} compound in k^{th} layer

Three main factors influence the path length of light in tissues: reflectance, scattering, and absorbance (Figure 14). Reflectance occurs at the surface of each layer, primarily at the interface between tissue and air. It is a function of refractive indices, which are nearly independent of wavelength. It can be reduced by applying oils to the skin. (2) (Figure 15). As the amount of oil increases, less light is reflected at the air tissue

interface to the detectors and the absorbance appears to increase. Note particularly the increase in the water band at 1510 nm relative to that at 1200 nm. The shape becomes more ideal. This is a physical effect, rather than an absorbance of the mineral oil. The absorbance increases for the hydrocarbon bands are observed at 1210 nm and in the 1700 nm region. Either dry skin or oil-based dressings can change reflectance.

Scattering (Rayleigh and Mie) occurs when light propagates through an inhomogeneous medium, such as skin, with its various types of cells, fibers and granules.(2) Rayleigh scattering describes effects seen when the wavelength is greater than the size of the inhomogeneities and Mie scattering describes the opposite case. Rayleigh scattering increase as the inverse of the fourth power of the wavelength (λ). Visible light (λ = 400-700 nm) is highly scattered by collagen fibers in the epidermis (Figure 16), though enough light reaches the capillaries in the dermis to make skin appear pink. NIR light (λ =700-1800 nm) is less scattered and may penetrate all layers of skin and some of the underlying muscle. Scattering is increased when proteins are denatured by heat. Hence cooked pork appears whiter than raw pork (Figure 17).

The effect of absorptivity on path length is more complex. Two photons with similar wavelengths might have similar trajectories based on scattering probabilities, but may have vastly different probabilities of being absorbed by tissues instead of being scattered to the spectrometer. The intensity of light decreases exponentially as light travels through the sample. This exponential decay is highly dependent on the absorptivities of the components in the sample. At any distance into the sample, the fraction of light remaining (T_j) is a function of both the path length already traveled (b_j) and the absorptivity of the sample (a_j).

$$T_j = e^{-(b*a)}$$

At some b_j, T_j will be approximately zero, and light will travel no further, or for reflectance, will be unable to return to the surface before being absorbed. The NIR absorptivity function of tissue closely resembles that of water (Figure 5), not surprising since tissues are about 80% water. Accordingly, 1460 nm light should be attenuated 17 times faster than 1100 nm light and 56 times faster than 1000 nm light. For pure water, an absorbance of 1.2 would correspond to path lengths of approximately 1.5 mm, 2 cm and 6 cm for these three wavelengths. In a scattering medium light propagates in random paths. Assuming that the absorptivity is the same, the total path length would be the same, but the penetration depth, the thickness of the sample the light travels through, would be less than half that. Figure 18 shows three thicknesses of muscle tissue. The apparent absorbance (-log(reflectance)) at 1460 nm increases only 20% when the thickness is increased from 0.5 to 1.0 mm, indicating that the penetration depth at this wavelength is about 0.6 mm. Absorbances between 900 and 1400 nm do increase in proportion to the thickness, indicating linear behavior at longer penetration depths, to at least 2.0 mm. Spectra in the visible region would show similar effects due to the strong absorbances of hemoglobins. Melanin also has strong absorbances in the visible region but is removed by initial debridement in burn wounds.

The large variability of penetration depths gives access to information not otherwise obtainable. Spectra between 500 and 600 nm reflect only the oxygenation levels of hemoglobin in the surface capillaries, not the tissues below. Light between 975 and 1100 nm reaches hemoglobins and myoglobins in the muscle tissues below the skin. 1150 nm light is absorbed primarily by water in the dermis and 1215 nm by fat in the layer below it. And light between 1400 and 1800 nm gives the hydration and collagen content of the surface layer, whether it is epidermis or exposed dermis.

This information can be further used to observe the development of scar tissue. Scars are composed primarily of collage fibers which scatter light and obscure spectra from the tissues below (Figure 19). It might be possible to correlate the increased

scattering and the "disappearance" of fat, hemoglobins and myoglobin absorbances with the thickness of scar tissue.

III. Models of Hemoglobin and Water Changes.

A. Ischemia -- deoxygenation of hemoglobin.

Introduction. Ischemia, deficient blood flow, occurs wherever circulation is restricted by mechanical means or by damage to blood vessels. The blood stagnates and turns blue as the surrounding tissues continue to use up the available oxygen. Eventually the tissues become deoxygenated and dysfunctional. This can be of great importance in partial thickness burns. A burn may initially appear to be shallow, but if the circulation has been damaged it develops ischemia and the skin dies, producing a full-thickness burn in a few days. There have been several instruments produced which can measure the oxygenation of blood spectroscopically (3) but they use probes that must contact the skin, and they require a strong blood flow at the site tested. Therefore, they are not applicable to either burn wounds or ischemia in general. With our non-contacting reflectance probe, however, it may be possible to determine the oxygenation of blood in a burn and to deduce whether it is sufficient to allow the wound to heal. Preliminary studies were done using an existing reflectance spectrophotometer which has a limited wavelength range (1100-1800 nm) which includes only a small fraction of the hemoglobin absorbances. We would expect better results using the wider range (450-1800 nm) which will be available when the LT instrument is fully functional.

Experimental. Ischemia was induced in a healthy forearm by applying a pressure cuff (150 mmHg) for 5 minutes. Spectra were taken in the NIR region (1100-1800 nm) every 30 seconds, using a Pacific Scientific 6250 spectrophotometer in reflectance mode. Then the pressure was released and circulation returned to normal. The second derivative spectra were analyzed by principle component

analysis (PCA), a multivariate statistical method which does not require independent measurement of constituent concentrations (4).

Results and discussion. Figure 20 shows the reflectance spectra taken during and after ischemia and figure 21 shows the same with the first spectrum subtracted. A continuous increase in the water band at 1460 nm is noted as well as large variations at 1100 nm which are due to oxy- and deoxy-hemoglobin and a smaller water band at 1150 nm. The second derivative spectra are shown in Figure 22. PCA resolves the derivative spectra into two components. The behavior of these components agrees with the known physiology of ischemia; when the circulation is restricted, the blood pools in the arm and becomes deoxygenated. When the restriction is released, the initial surge of new blood causes an oxygenation "overshoot" which gradually returns to normal equilibrium (5). Figure 23 shows the first spectral factor (loading) extracted by PCA. The scores (estimated concentrations) for this factor are given in Figure 24. The continuous increase of the scores and the spectral band at 1460 nm (water) in the loading correlate to the expected increase in blood. The loading and scores for the second factor (Figures 25 and 26) correspond to the change in the ratio of oxy- and deoxy-hemoglobin, though it's somewhat distorted because the blood concentration and the oxygenation ratio are not strictly independent.

From this experiment, it is clear that we are able to observe and interpret small spectral changes related to the concentration and oxygenation level of hemoglobin in tissue *in vivo*. This can be done non-invasively, without contacting the subject, and may prove to be a valuable tool for burn depth analysis.

B. Basic Studies of Water Spectra.

Many models of water explaining different features of the spectra exist in the literature. Nevertheless the development of the new low noise NIR-spectrophotometers combined with multivariate statistics, state of the art mathematical tools, provides an impetus for restudy of the spectra of the pure water as a function

of temperature. In the spectral region 850-1100 nm water spectra exhibit an intense combination band centered near 967 nm. This peak demonstrates a strong dependence on the temperature. We have carried out spectroscopic studies of the 850-1100 nm region with a Pacific Scientific (PSCo) spectrometer. The measurements were made with 1 cm optical path length cell. Temperature control was achieved by equilibrating the samples cells in a water bath at a fixed temperature. The reported temperatures are believed to be correct to within 0.5 °C. The spectra from the PSCo spectrometer are shown in Figure 27 for the temperature range 10-80 °C. The spectra contain some noise and baseline offset due to scattering and refractive index changes. The slope and offset can be eliminated by calculating the 2nd derivative or normalization of the spectra by subtracting the offset and the slope. The 2nd derivative of the absorbance and normalized spectra are plotted in Figures 28 and 29 respectively. The difference spectra, when the "coldest" spectrum is subtracted from all others is shown in the Figure 30. These spectra are helpful for understanding the structure of the combination band peaks and can give us an idea how many different species (peaks) water spectra contain. The subject of specific interest was the band at 967 nm, assigned to the $2v_1+v_3$ second overtone of water. The multivariate statistic analysis for these spectra in the spectral range 850-1100 nm, with the aid of PLS (Partial Least Squares), PCA (Principal Component Analysis), and EFA (Evolving Factor Analysis) suggest that the data can be described by three latent variables. Assuming a mixture model for water, that implies that there are three molecular species in pure water whose proportion varies systematically with temperature. The results of Evolving Factor Analysis are shown in Figure 31. This picture shows the order of magnitude of the singular values vs constituent variable (temperature) in a logarithmic scale. Each curve corresponds to a single eigenvector. We can deduce from this picture that the data can be described by three eigenvectors, that are well defined above the noise. The loadings(spectral eigenvectors) and scores (titration eigenvectors) found from PCA

analysis are shown in Figures 32 and 33. For the purpose of understanding what are the real spectra and their weights in the resulting peak, we have to rotate the eigenvectors so that (a) the spectra would all be positive and (b) the thermal behavior follows the assumption of thermodynamic equilibrium, which is affected by temperature. We are currently developing a program to carry this rotation and derive the pure spectra and H_j's, the energies of hydrogen bond formation.

CONCLUSIONS AND SUGGESTIONS FOR FURTHER STUDY

We have developed instrumentation and apparatus which is capable of obtaining reflectance spectra of live human subjects in the wavelength region 900-1800 nm. Studies of the basic biochemicals and constituents of tissue have led to an understanding of the spectral peaks exhibited by human tissue. We have assigned these peaks to specific species. Water is the largest absorber in human tissue and therefore careful attention was paid to its spectroscopy. The near-infrared spectrum of water is very temperature dependent but can be described by a model which invokes only three species which differ in their hydrogen bonding properties. These results appear to be applicable to understanding changes in human physiology as evidenced by studies of pressure cuff induced ischemia in volunteers.

In the next year, we plan to (1) continue our studies of pure water. (Our goals are to understand temperature effects, perhaps to measure temperature non-invasively, and to investigate whether changes in the water spectrum reflect tissue hydration/denaturation effects.) (2) extend the spectral range to the visible range. (This will allow us to observe the hemoglobins, perhaps distinguishing oxy, deoxy, CO and met forms.) and (3) initiate studies of patients in the Harborview Burn Center.

References

1) *Near-Infrared Technology in the Agricultural and Food Industries*; Williams,P.; Norris,K., Eds.; American Association of Cereal Chemists: St.Paul, MN, 1987; Chapter 2.

2) Anderson,R.R; Parrish,J.A.; *J.Invest.Dermatol.* **1981**, *77*, 13-19.

3) Yelderman,M.; *Anesthesiology*, **1984**, *61*, A164.

4) Beebe,K.R.; Kowalski,B.R.; *Anal.Chem.* **1987**, *59*, 1007A-1017A.

5) Hampson,N.B.; Piantodosi,C.A. *J.Appl.Physiol.* **1988**, *64(6)*, 2449-2347.

TABLE I.

E. Table of Assignments.

1764	Fat	CH_2 stretch, 1st overtone
1731	Fat	CH_2 stretch, 1st overtone
1728	Collagen	
1708	Fat	CH_3 stretch, 1st overtone
1689	Collagen	
1460	Water (0th derivative)	OH stretch, 1st overtone
1400	Water (2nd derivative)	
1275	Collagen?	
1213	Fat	CH_3 stretch, 2nd overtone
1189	Fat	CH_3 stretch, 2nd overtone
1188	Protein in muscle tissue	
1153	Water	OH combination
1038	Fat	CH_2 combination
1014	Fat	CH_3 combination
958	Water	OH stretch, 2nd overtone
929	Fat	CH_2 stretch, 3rd overtone
760	Deoxyhemoglobin	
576	Oxyhemoglobin	
555	Deoxyhemoglobin	
541	Oxyhemoglobin	

Instrument Baseline Noise

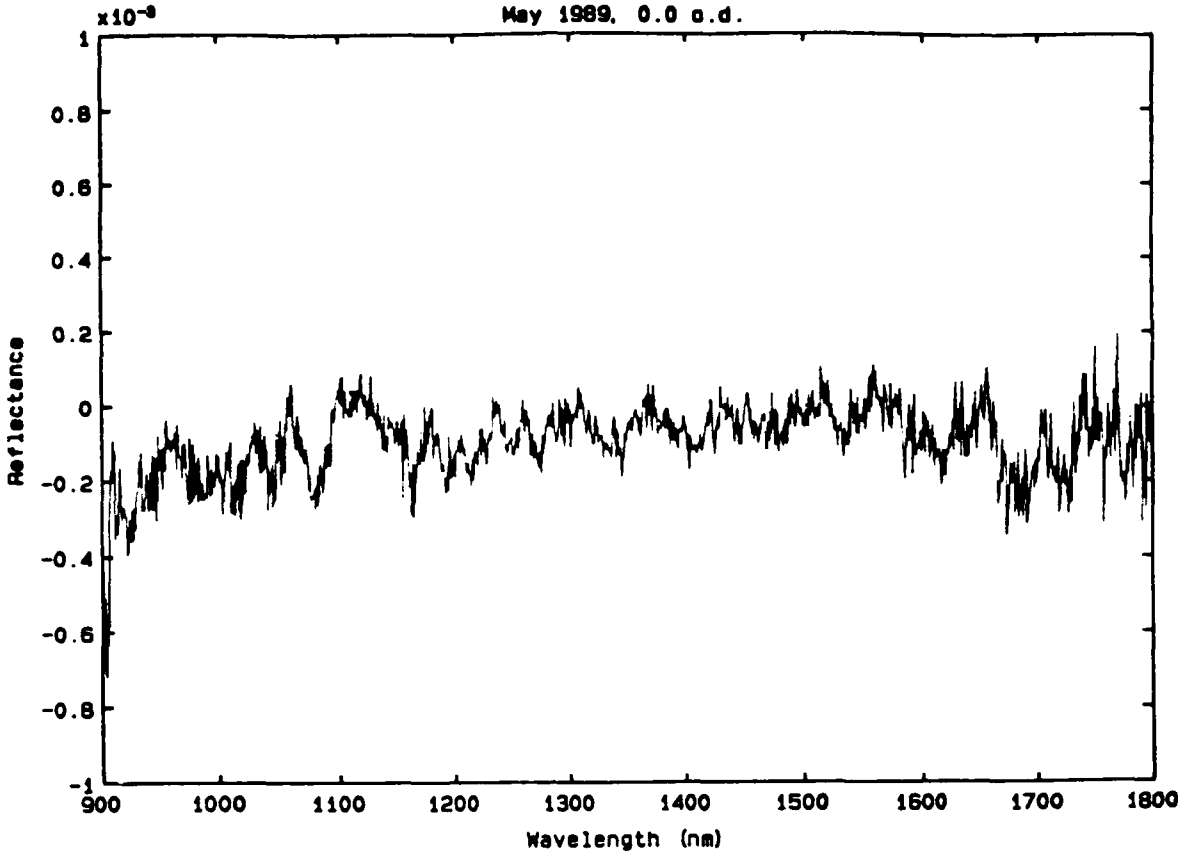

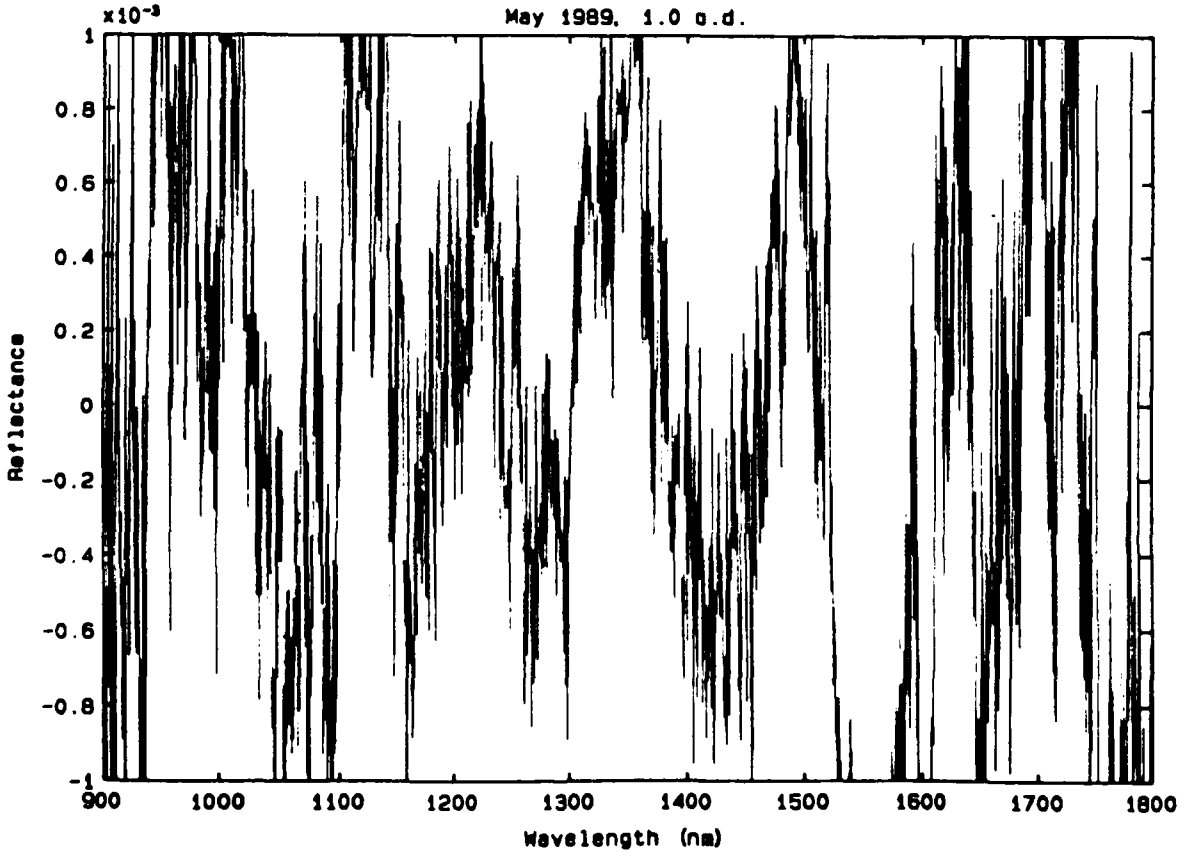

Figure 1

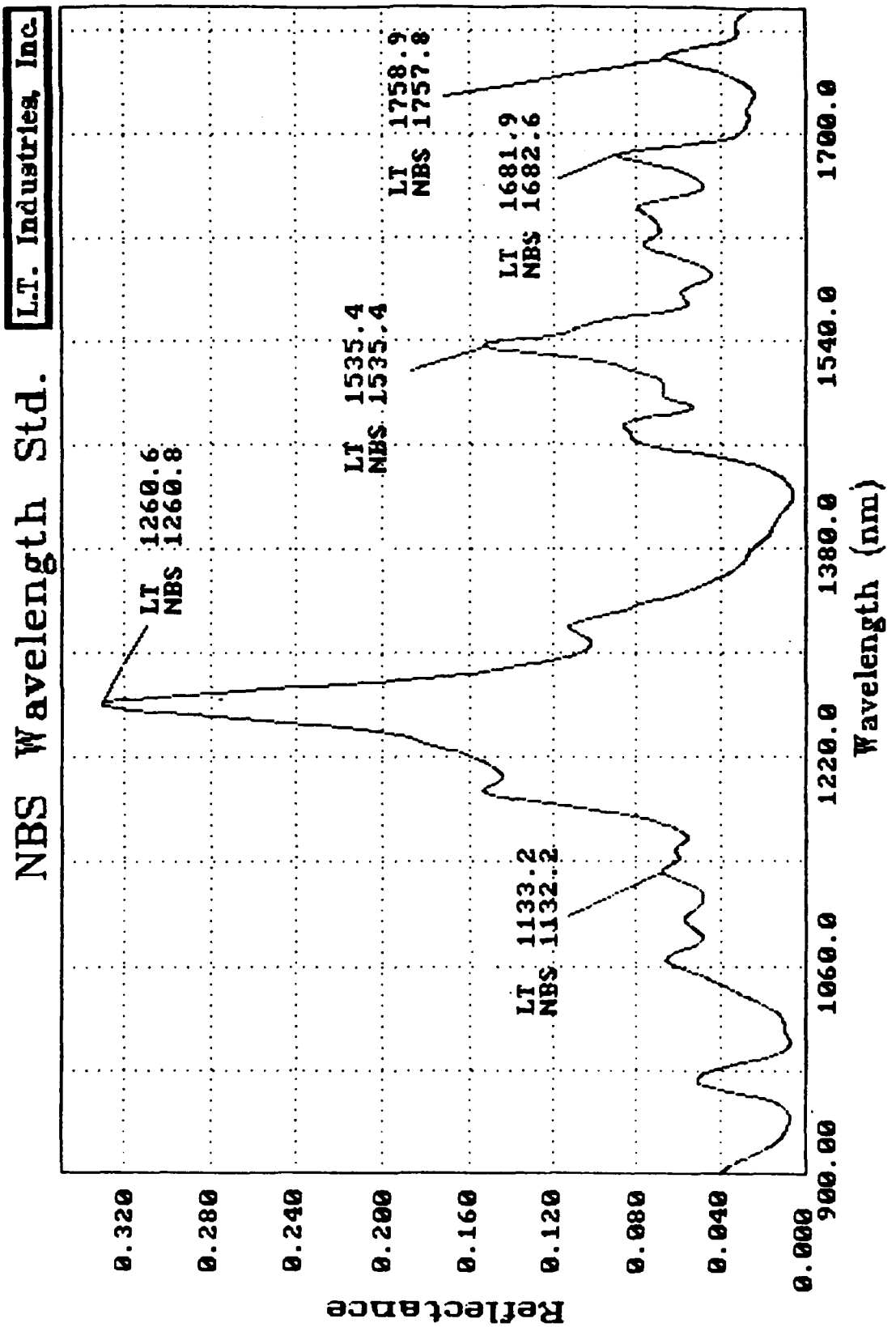
NBS Wavelength Std.
LT. Industries, Inc.
LT 1260.6
NBS 1260.8
LT 1535.4
NBS 1535.4
LT 1681.9
NBS 1682.6
LT 1758.9
NBS 1757.8
LT 1133.2
NBS 1132.2
Reflectance
0.320
0.280
0.240
0.200
0.160
0.120
0.080
0.040
0.000
900.00
1060.0
1220.0
1380.0
1540.0
1700.0
Wavelength (nm)

Figure 2

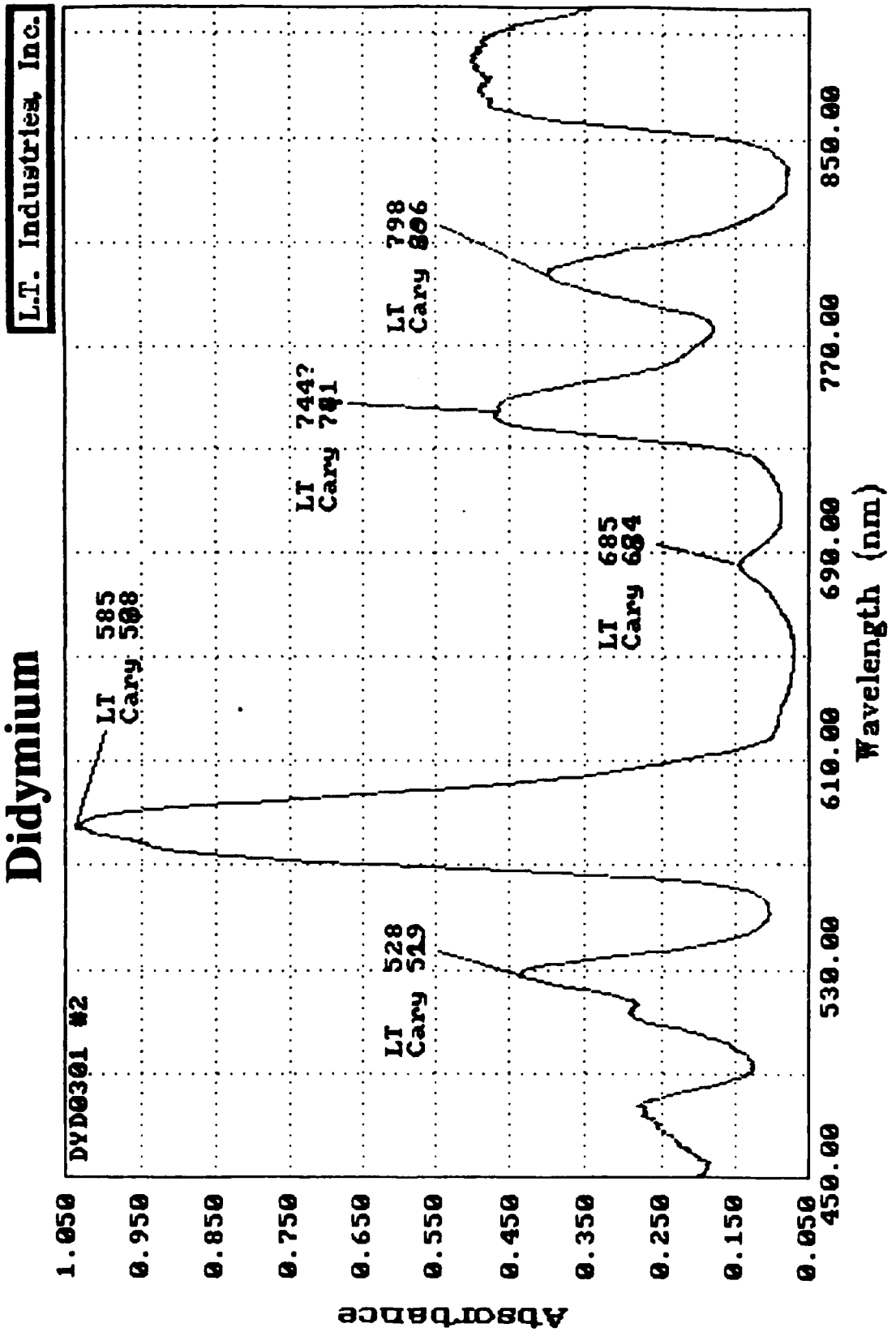
Didymium
L.T. Industries, Inc.
DYD0301 #2
LT 585
Cary 588
LT 528
Cary 529
LT 744?
Cary 741
LT 685
Cary 684
LT 798
Cary 806
Absorbance
1.050
0.950
0.850
0.750
0.650
0.550
0.450
0.350
0.250
0.150
0.050
450.00
530.00
610.00
690.00
770.00
850.00
Wavelength (nm)

Figure 3

Second Derivative Transformations

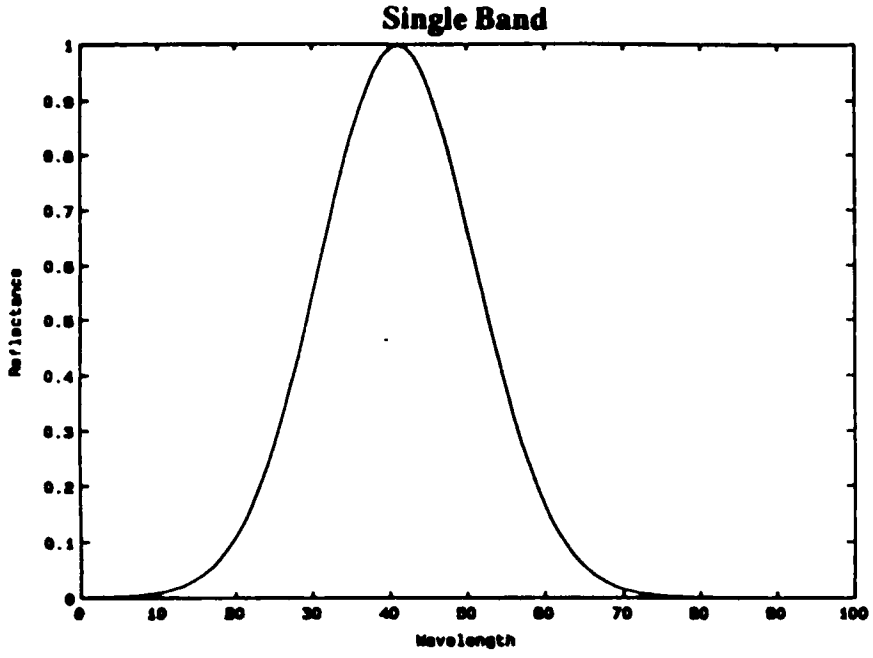

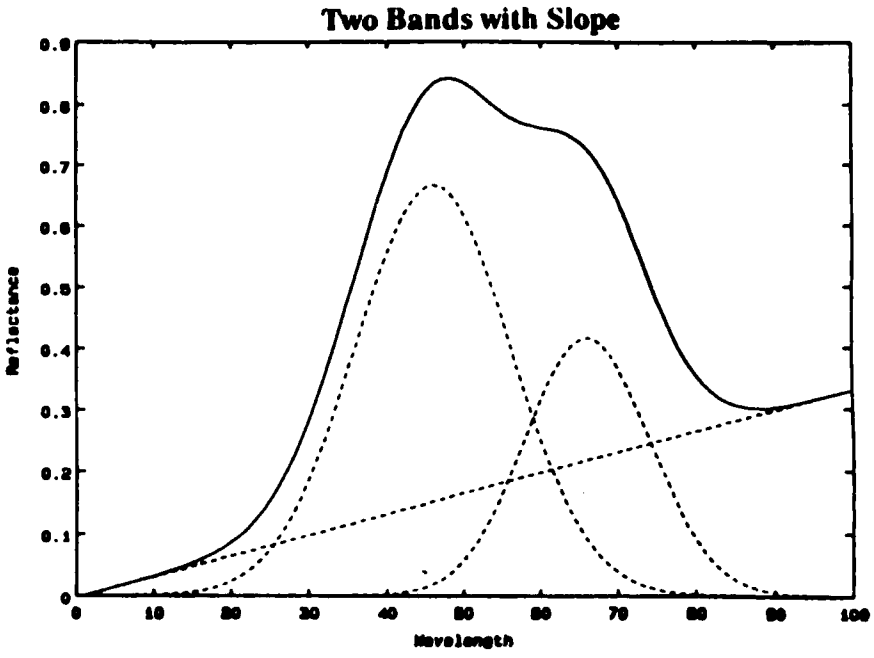

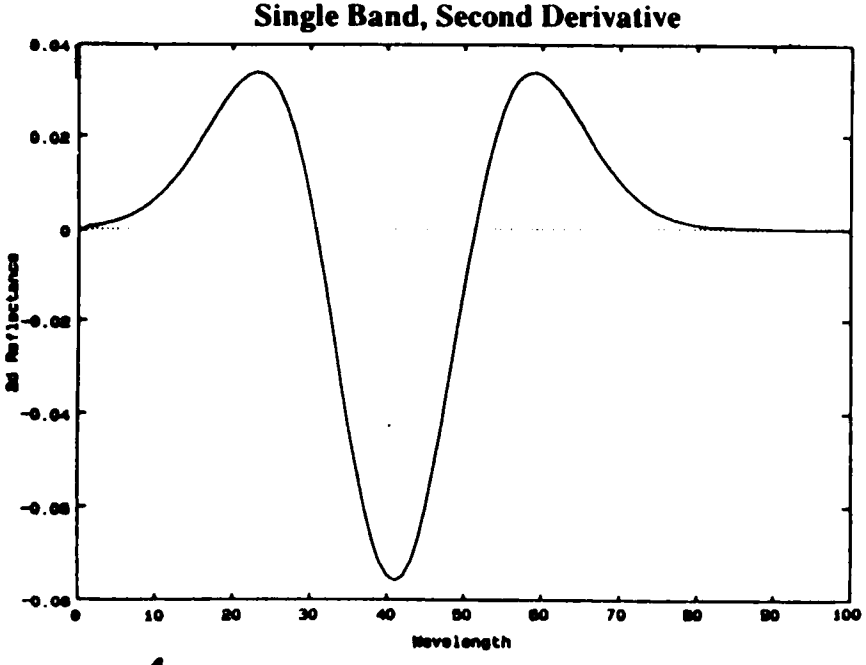

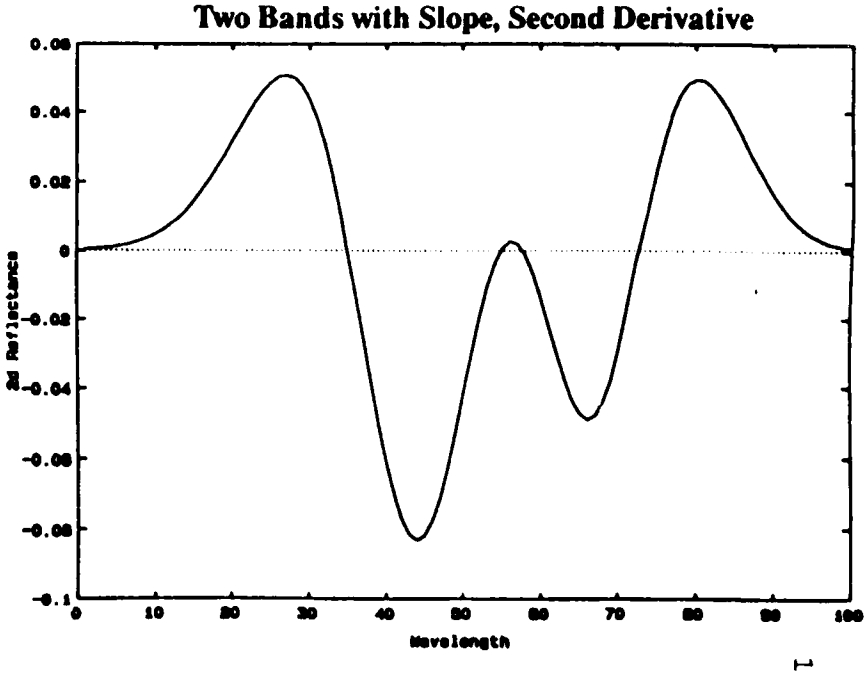

Figure 4

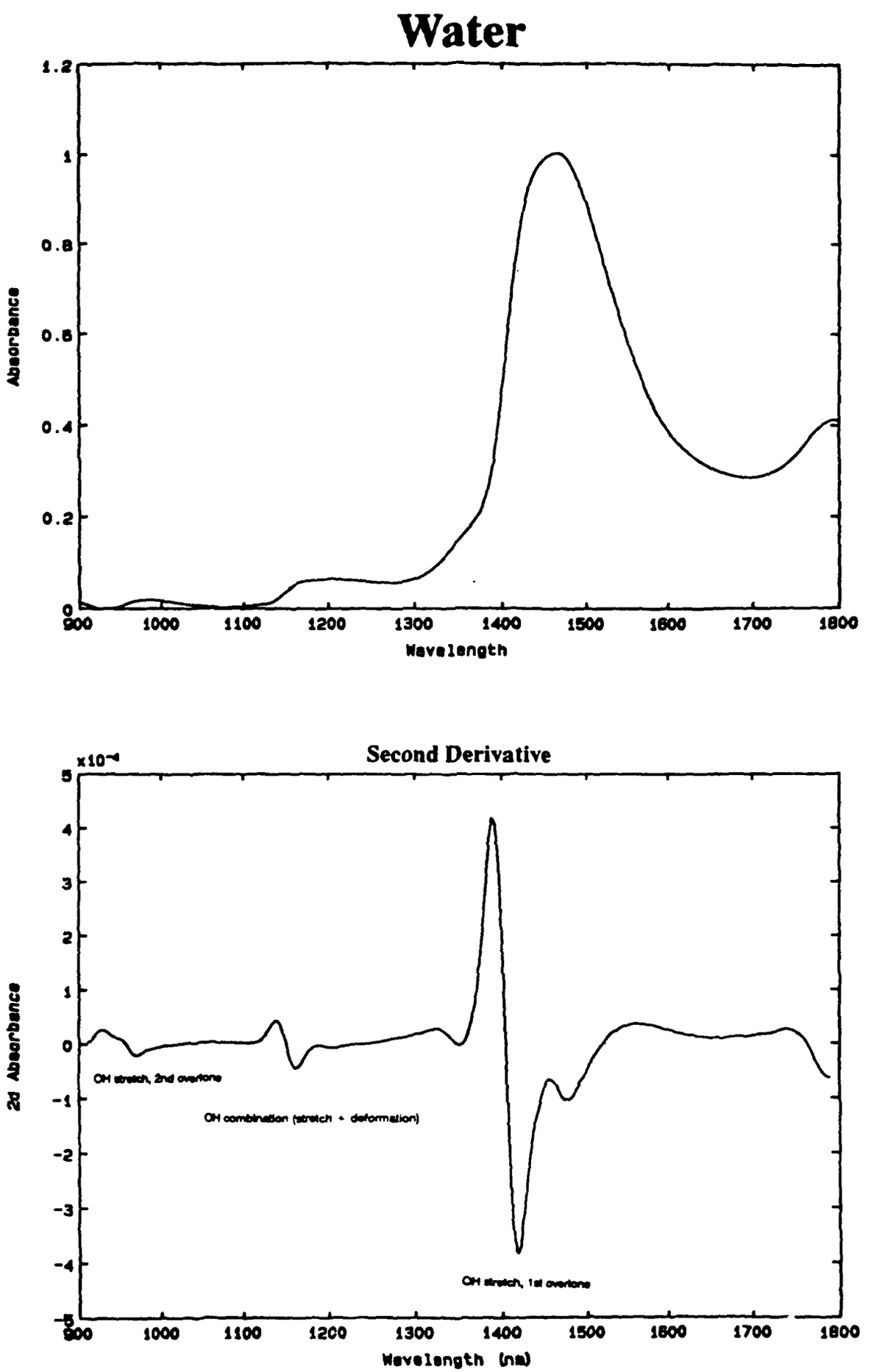
Water
Absorbance
Wavelength
Second Derivative
2d Absorbance
OH stretch, 2nd overtone
OH combination (stretch + deformation)
OH stretch, 1st overtone
Wavelength (nm)

Figure 5

Mineral Oil

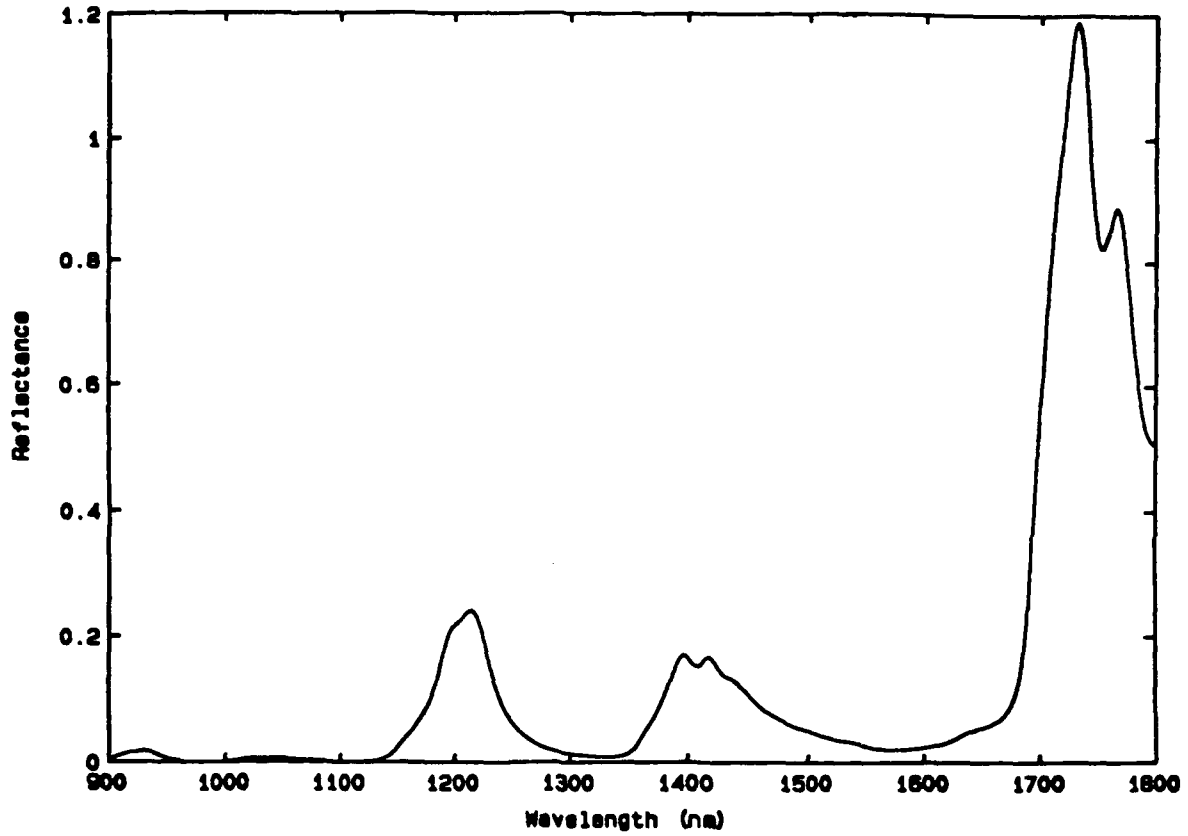

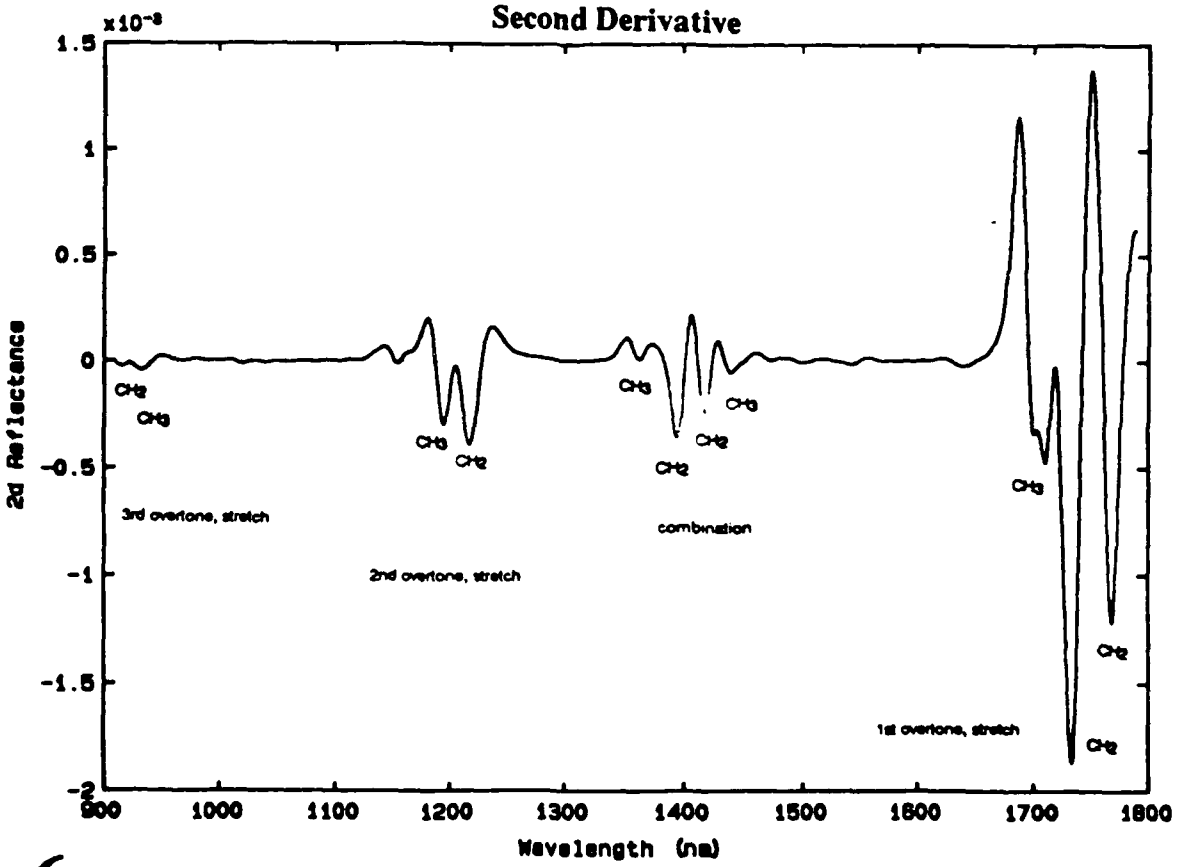

Figure 6

Collagen

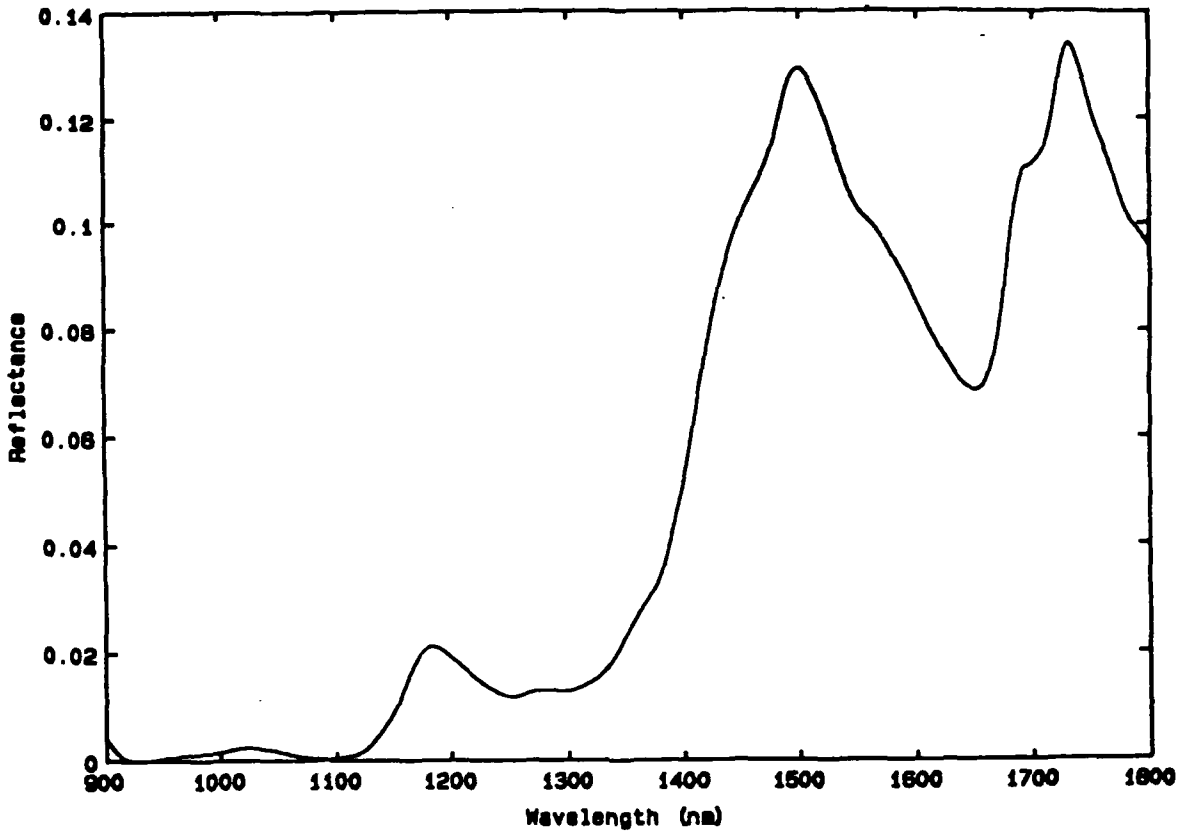

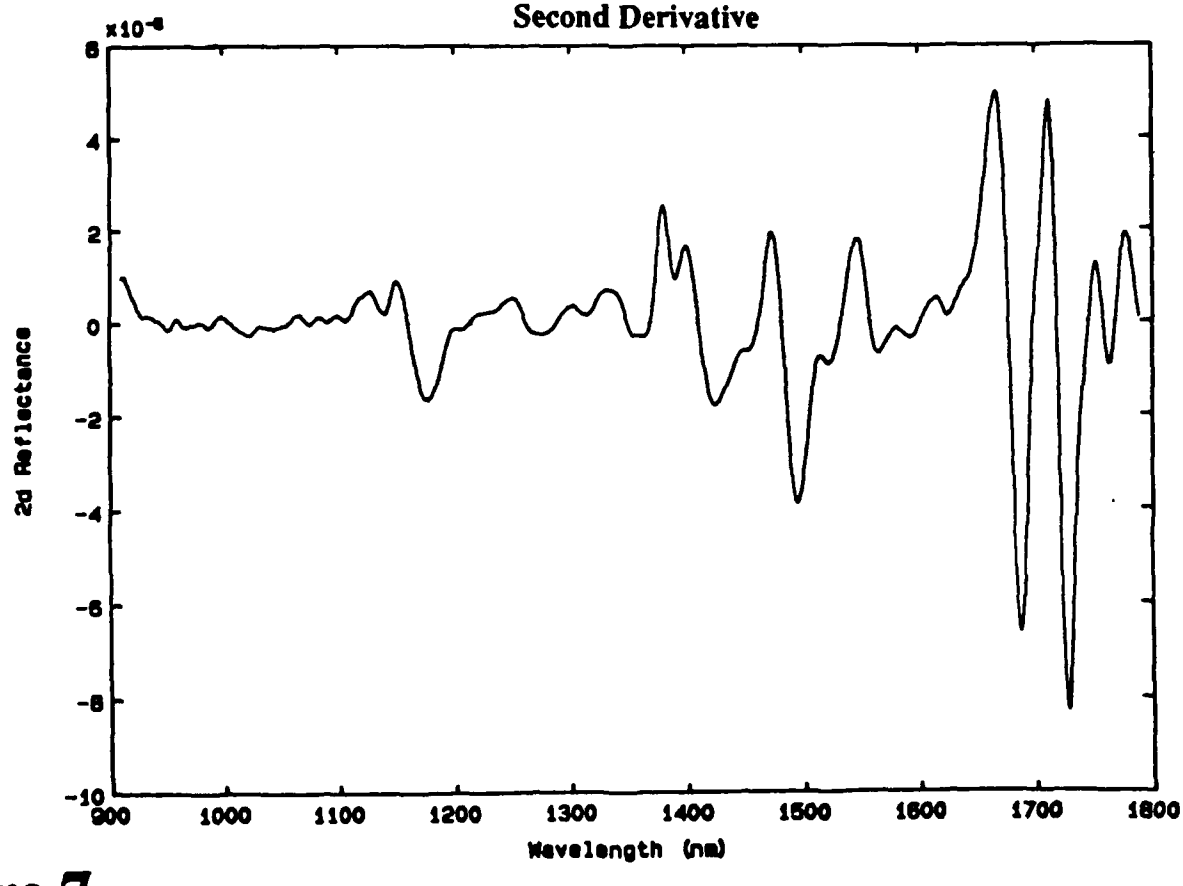

Figure 7

Fat

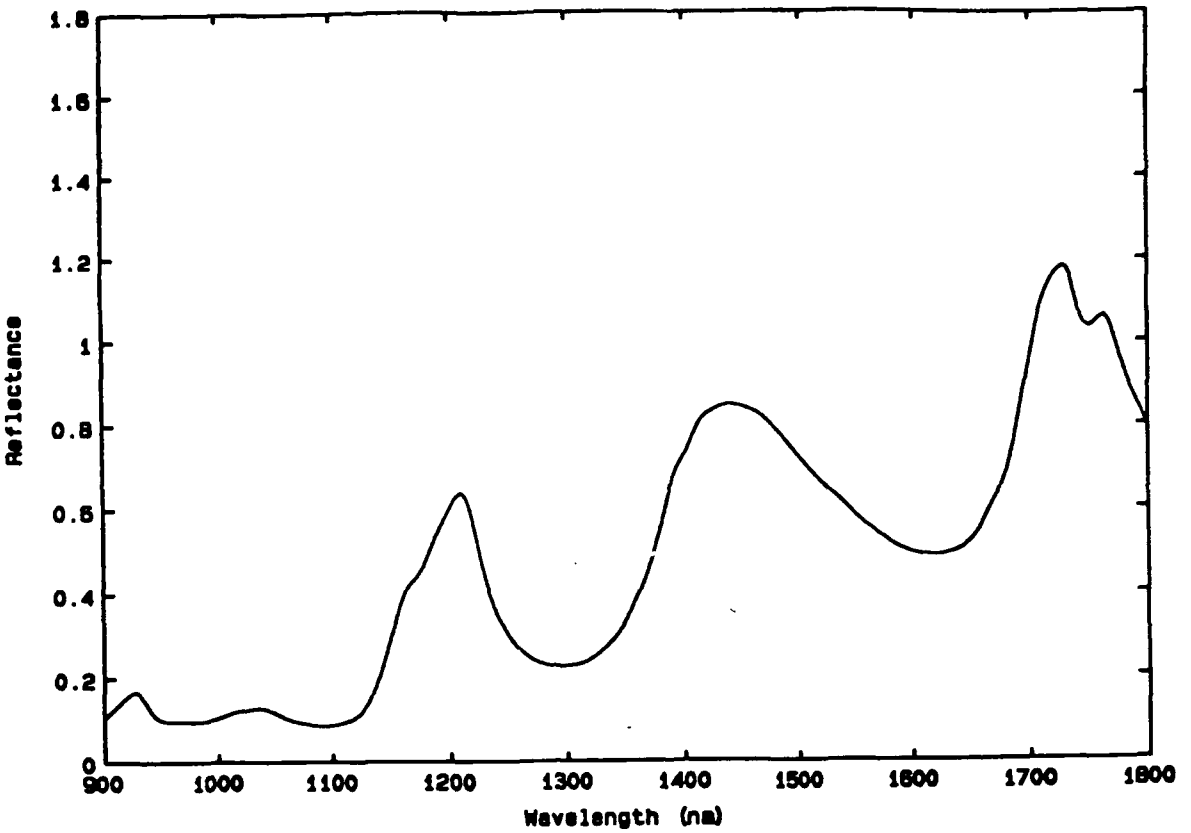
Reflectance
Wavelength (nm)

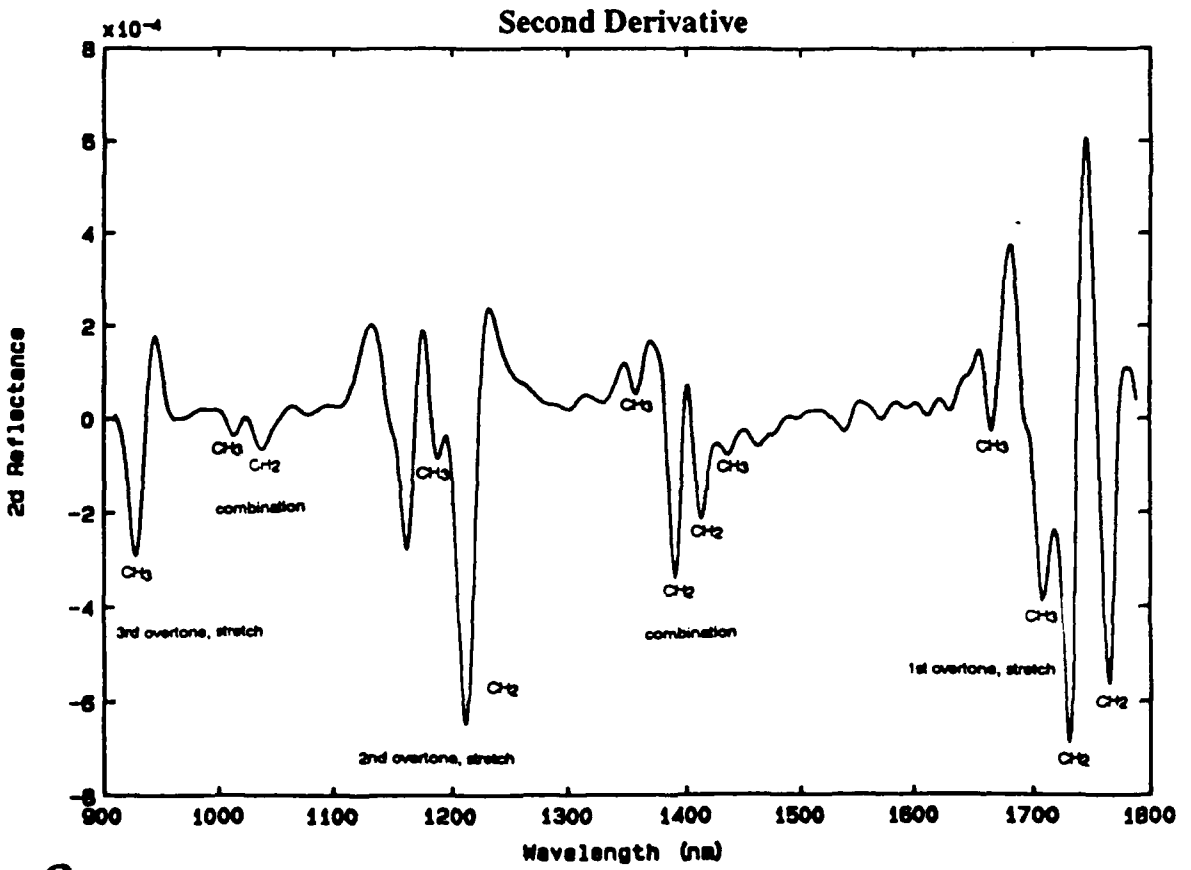
Second Derivative
x10⁻⁴
2d Reflectance
Wavelength (nm)
CH3
CH2
combination
3rd overtone, stretch
2nd overtone, stretch
1st overtone, stretch

Figure 8

Muscle Tissue

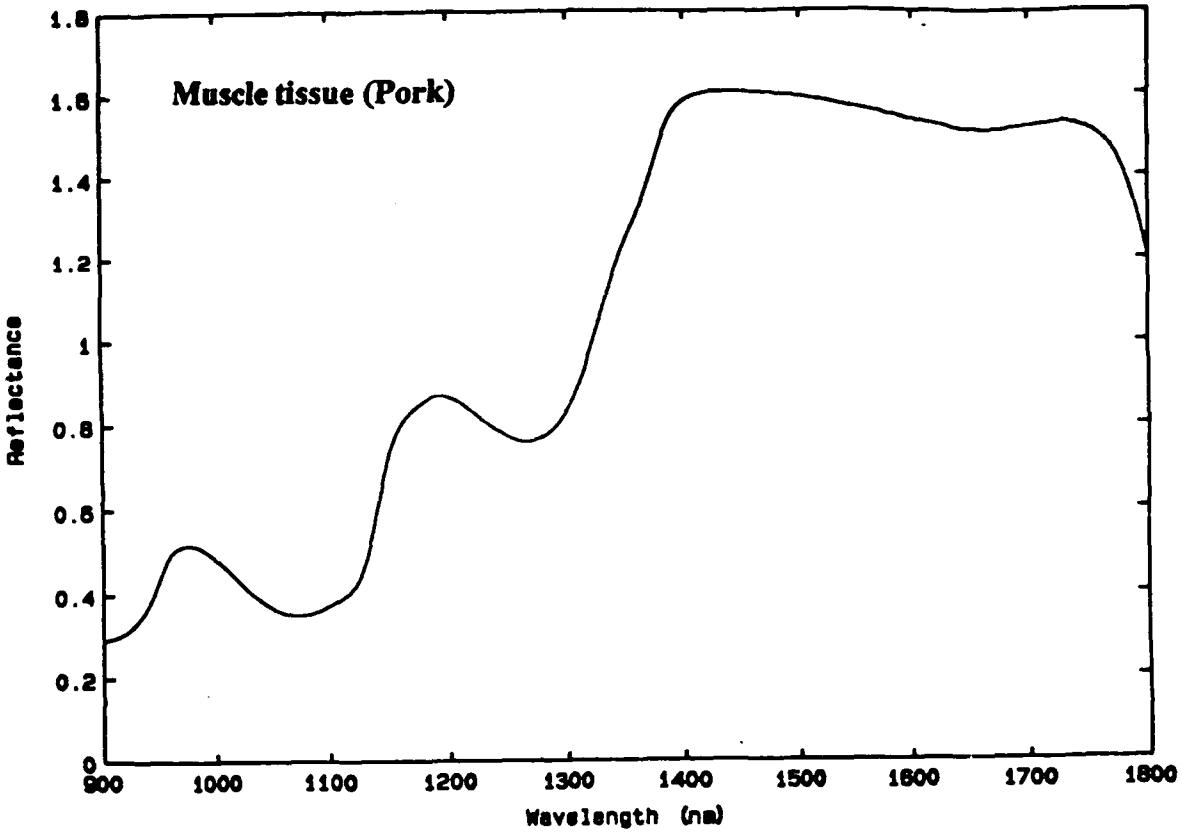

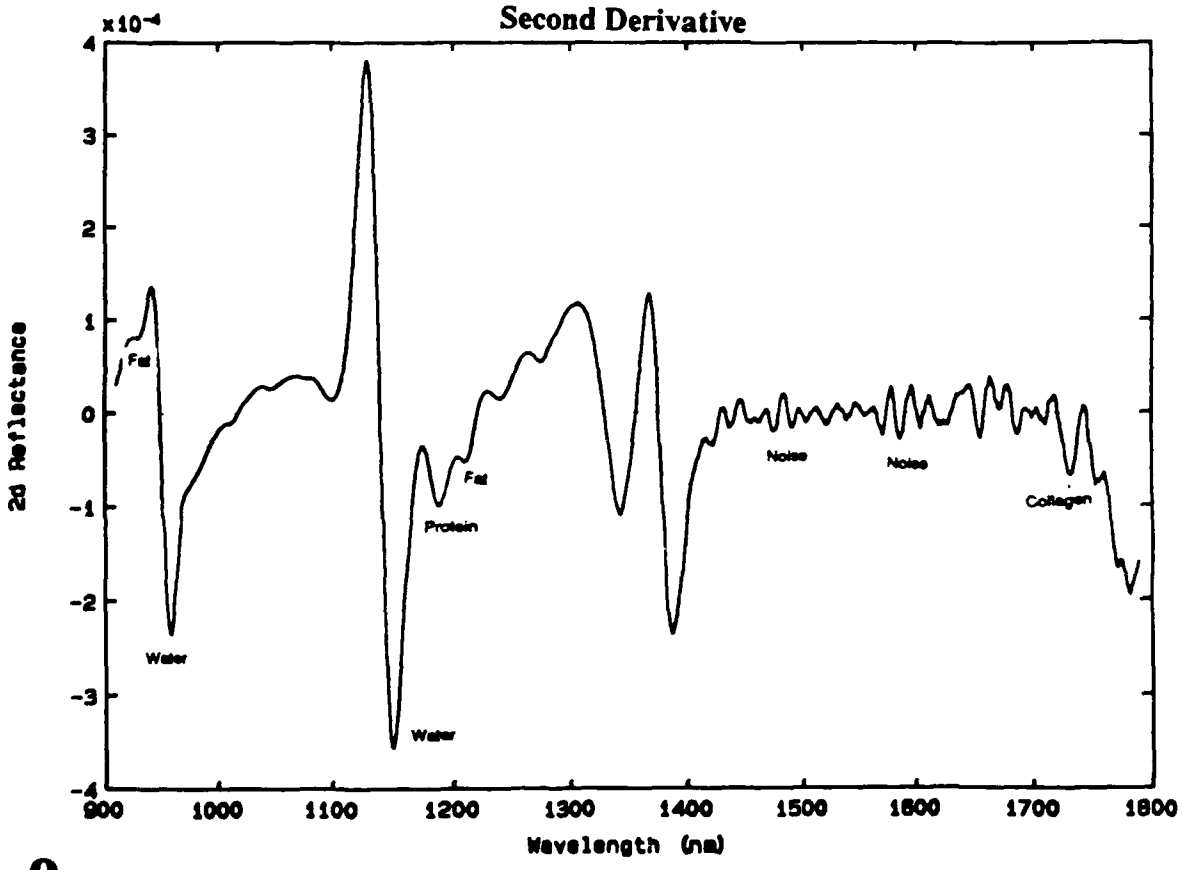

Figure 9

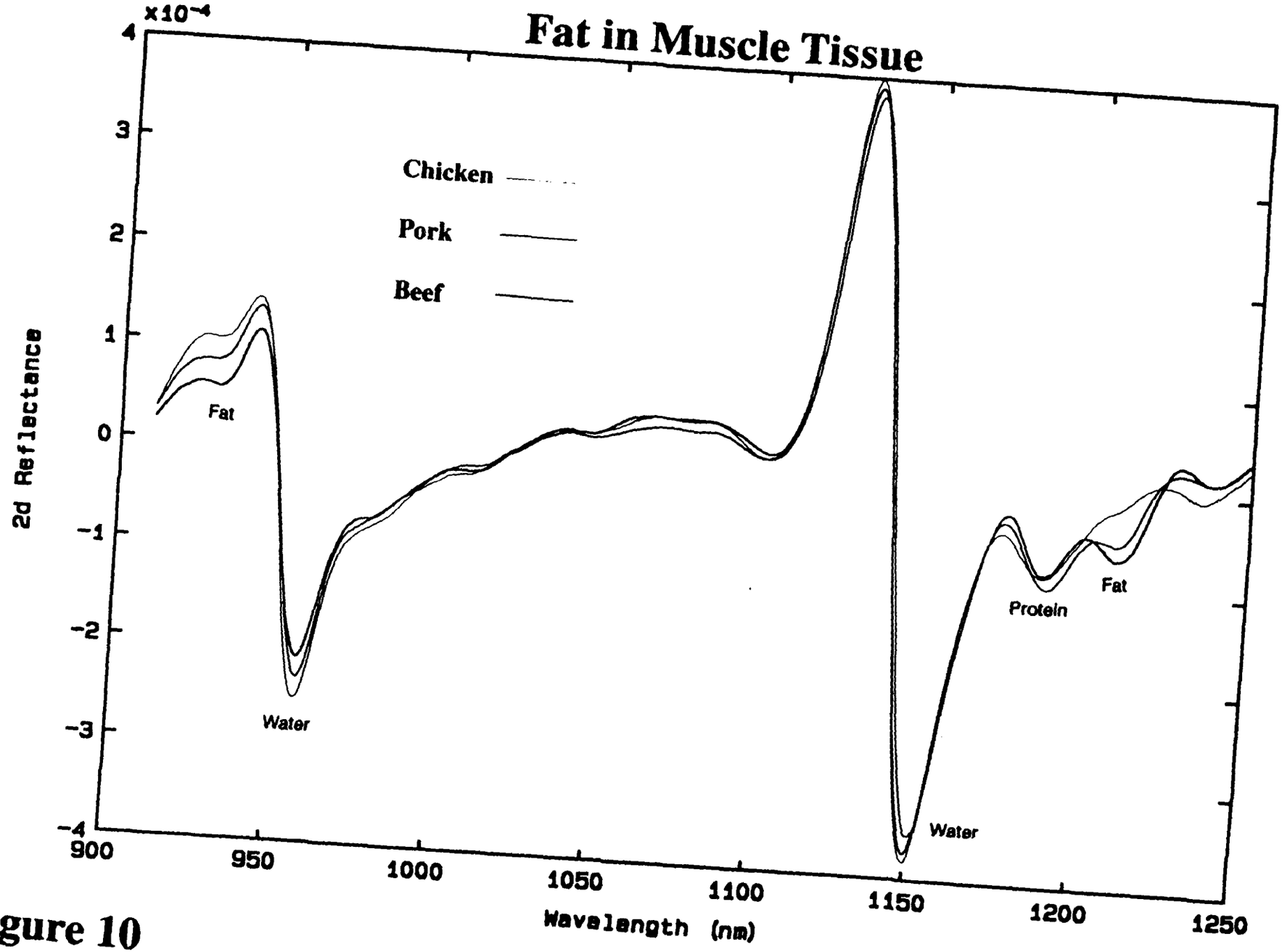
Fat in Muscle Tissue
x10⁻⁴
4
3
2
1
0
-1
-2
-3
-4
2d Reflectance
Chicken
Pork
Beef
Fat
Water
Protein
Fat
Water
900
950
1000
1050
1100
1150
1200
1250
Wavelength (nm)

Figure 10

Tendon

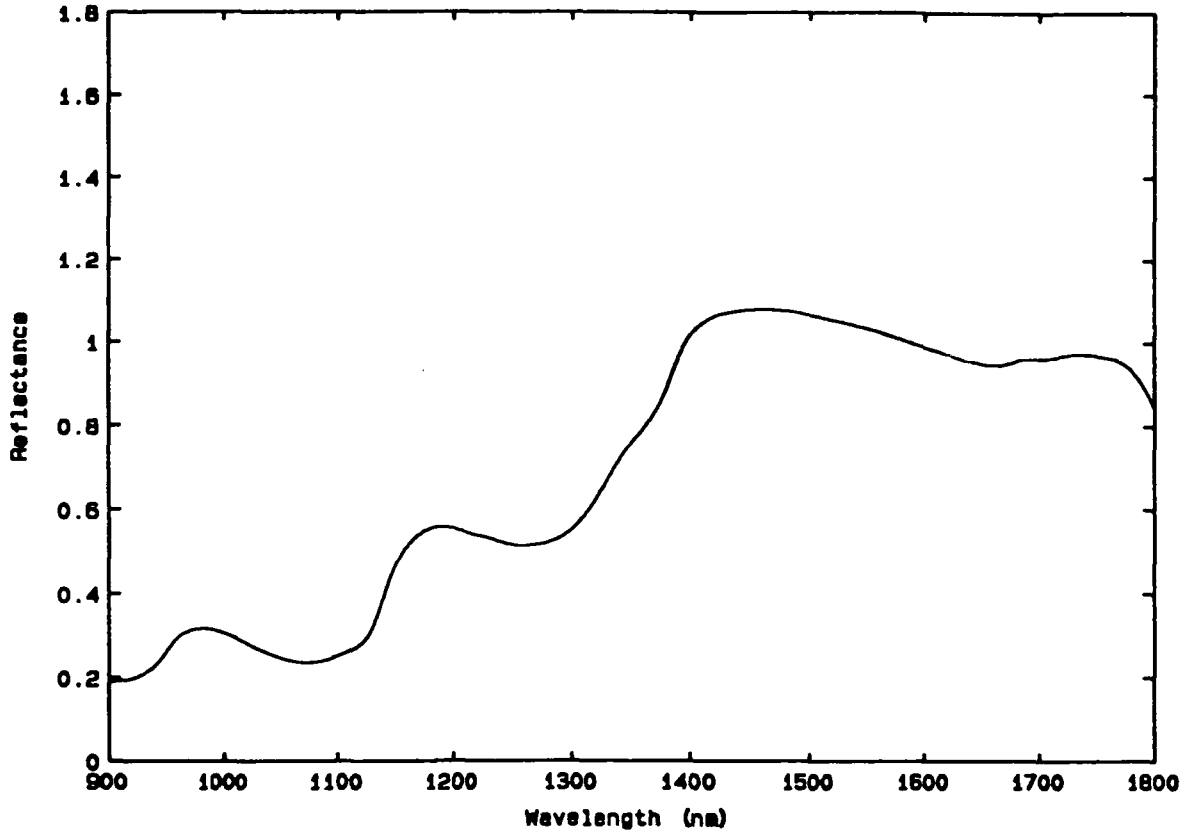

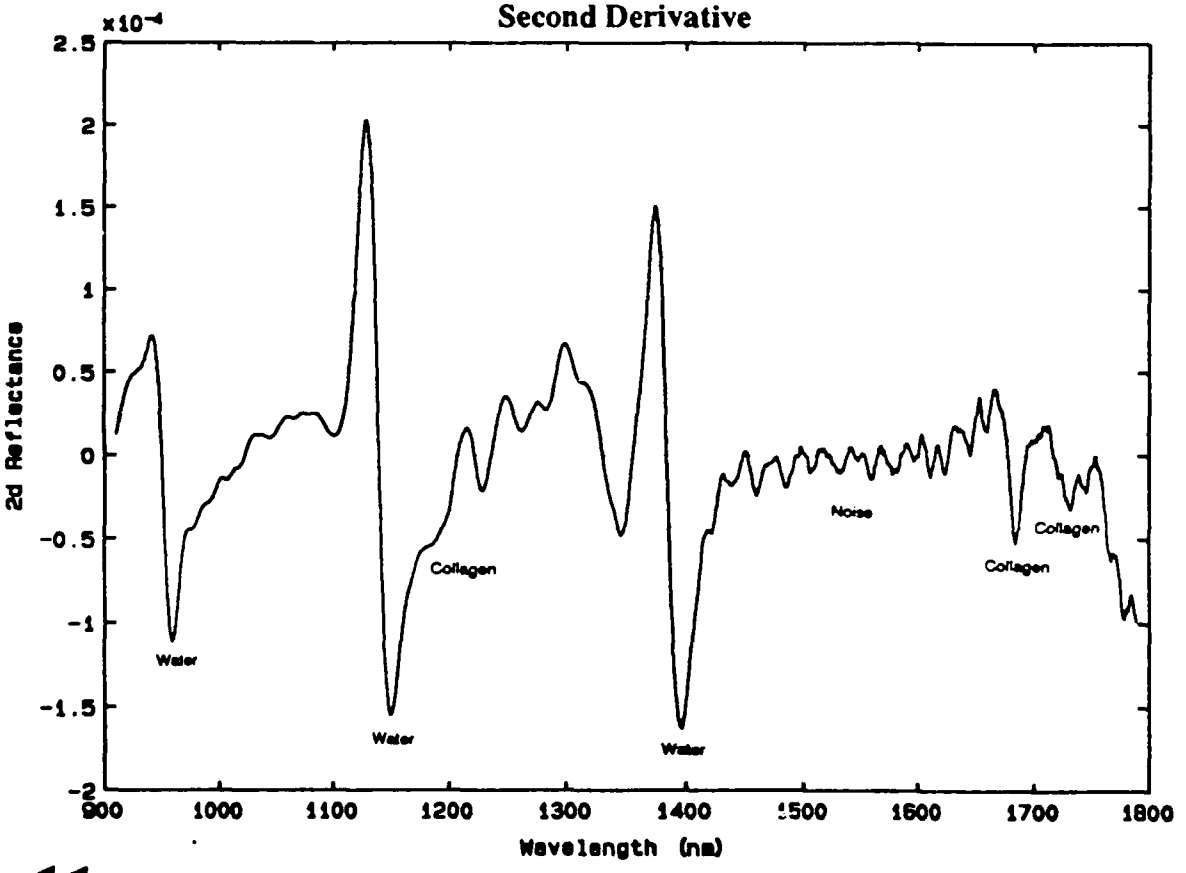

Figure 11

Skin excised, Rat

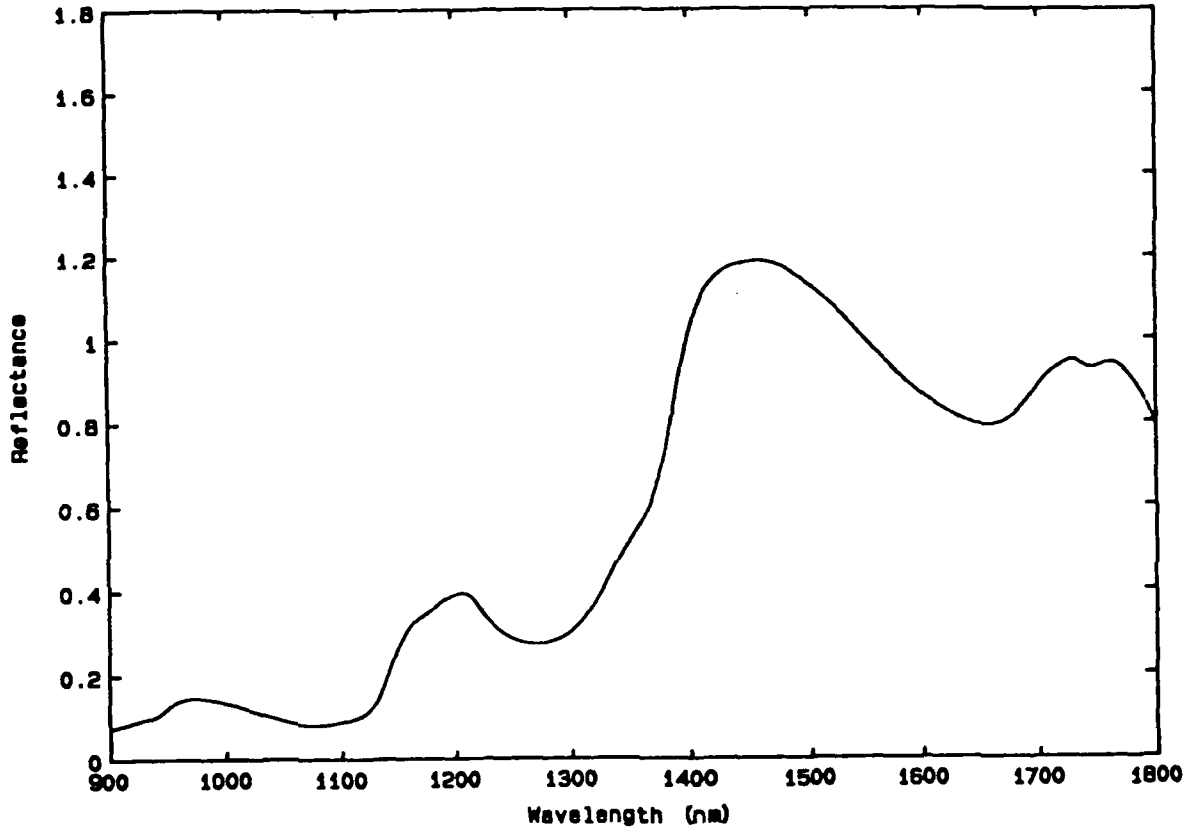

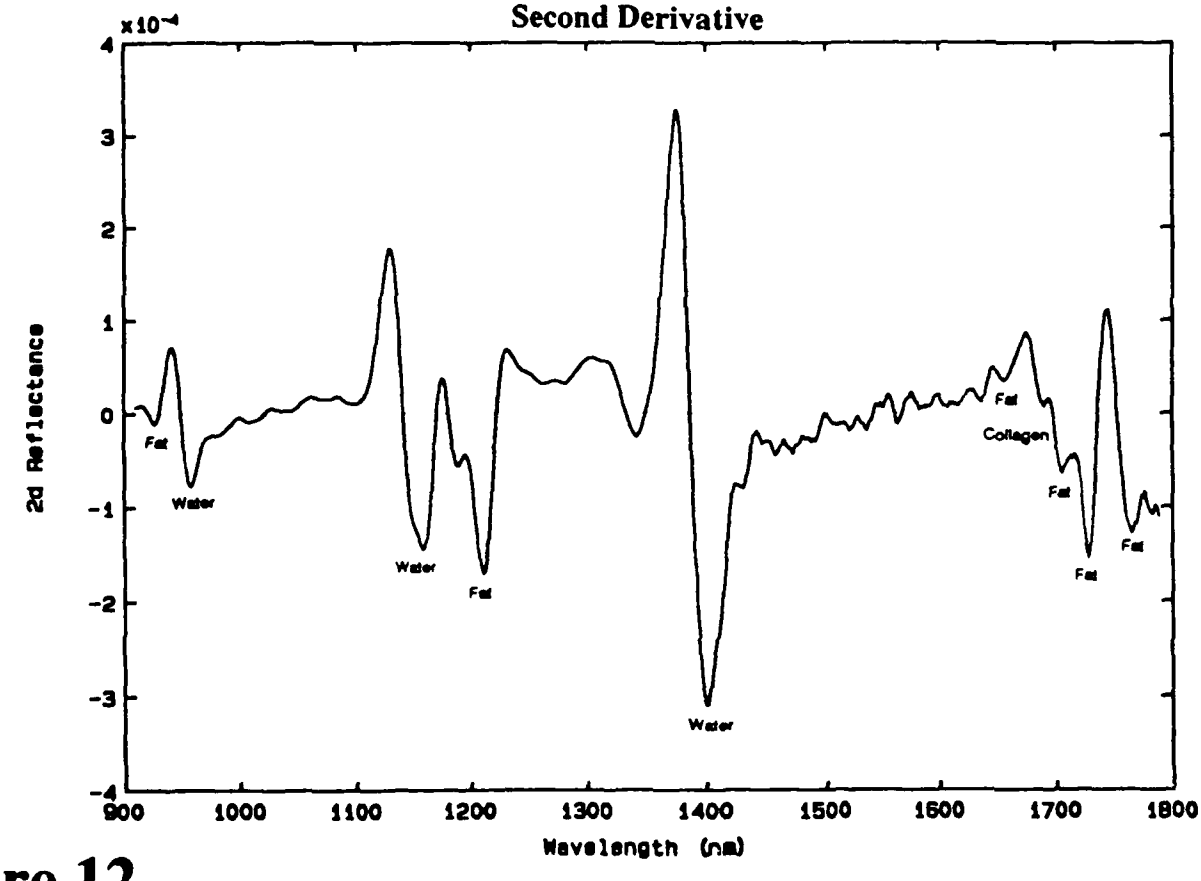

Figure 12

Skin in vivo, Human

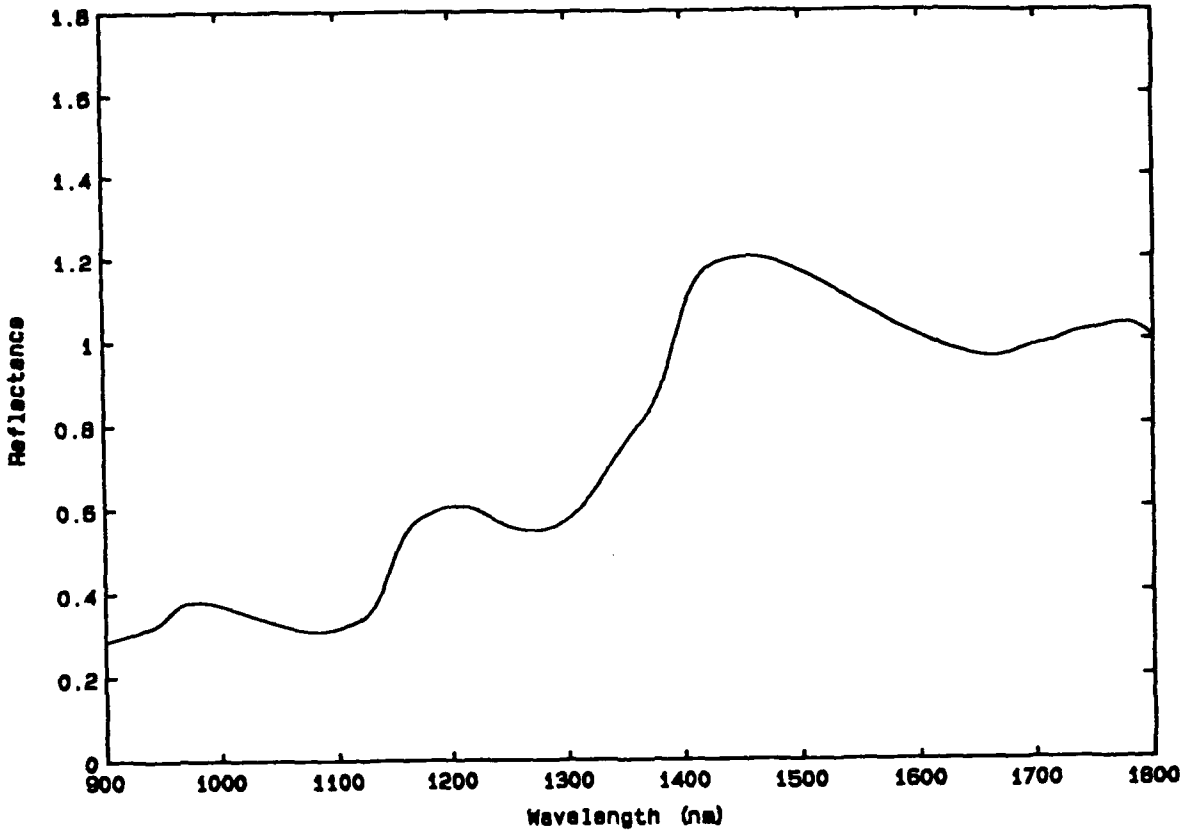

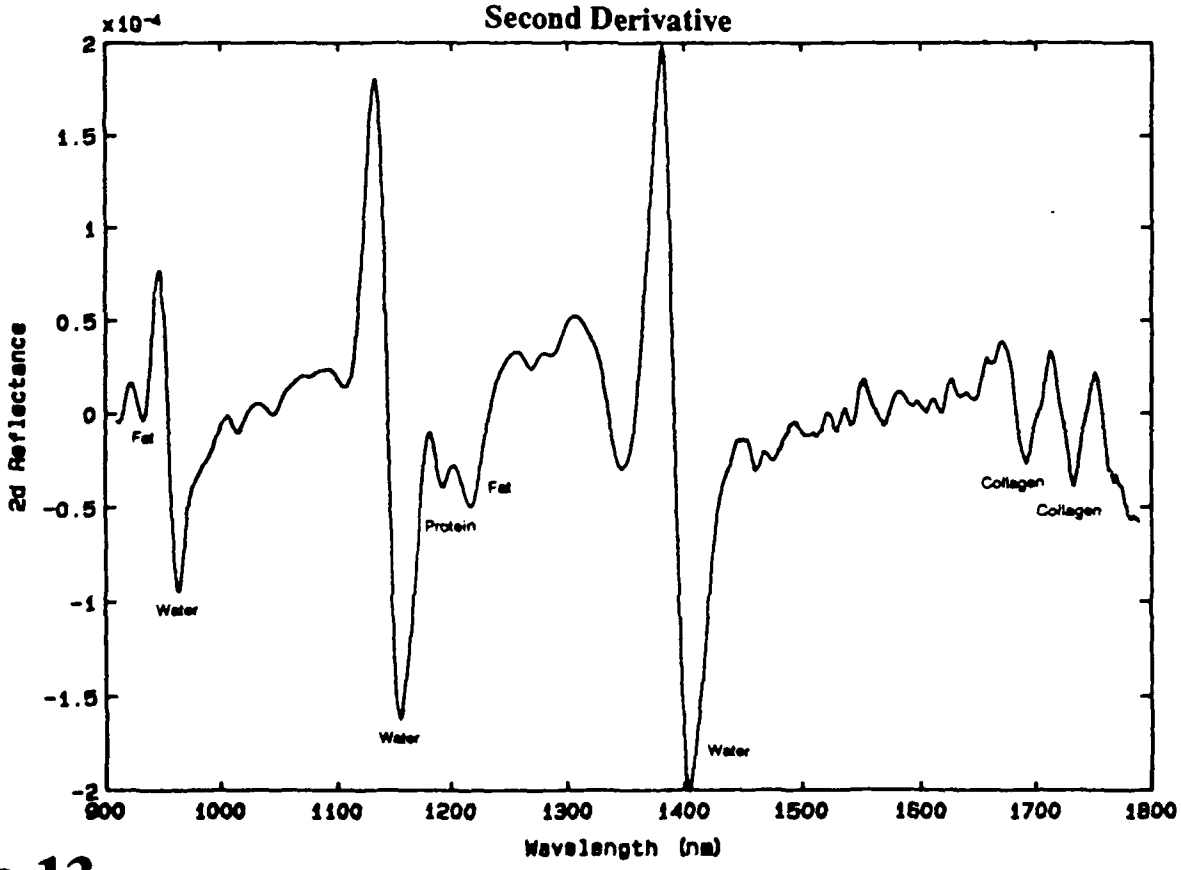

Figure 13

Reflectance, Absorbance, and Scattering

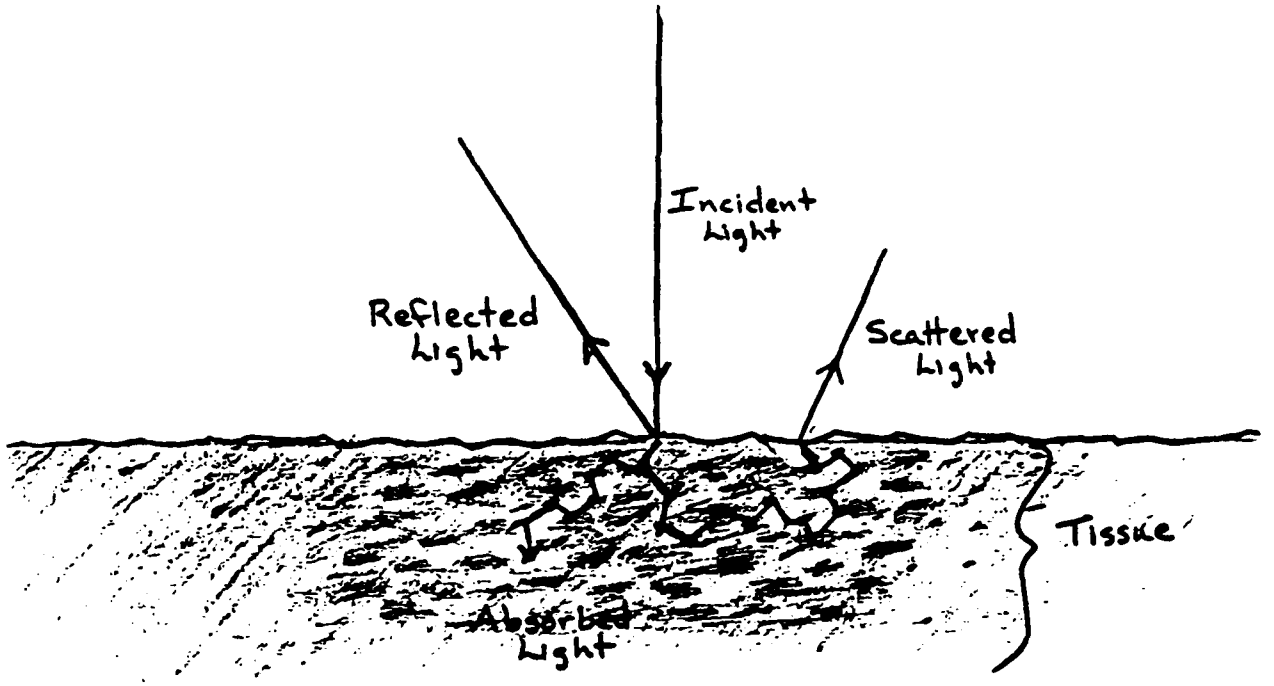

Figure 14

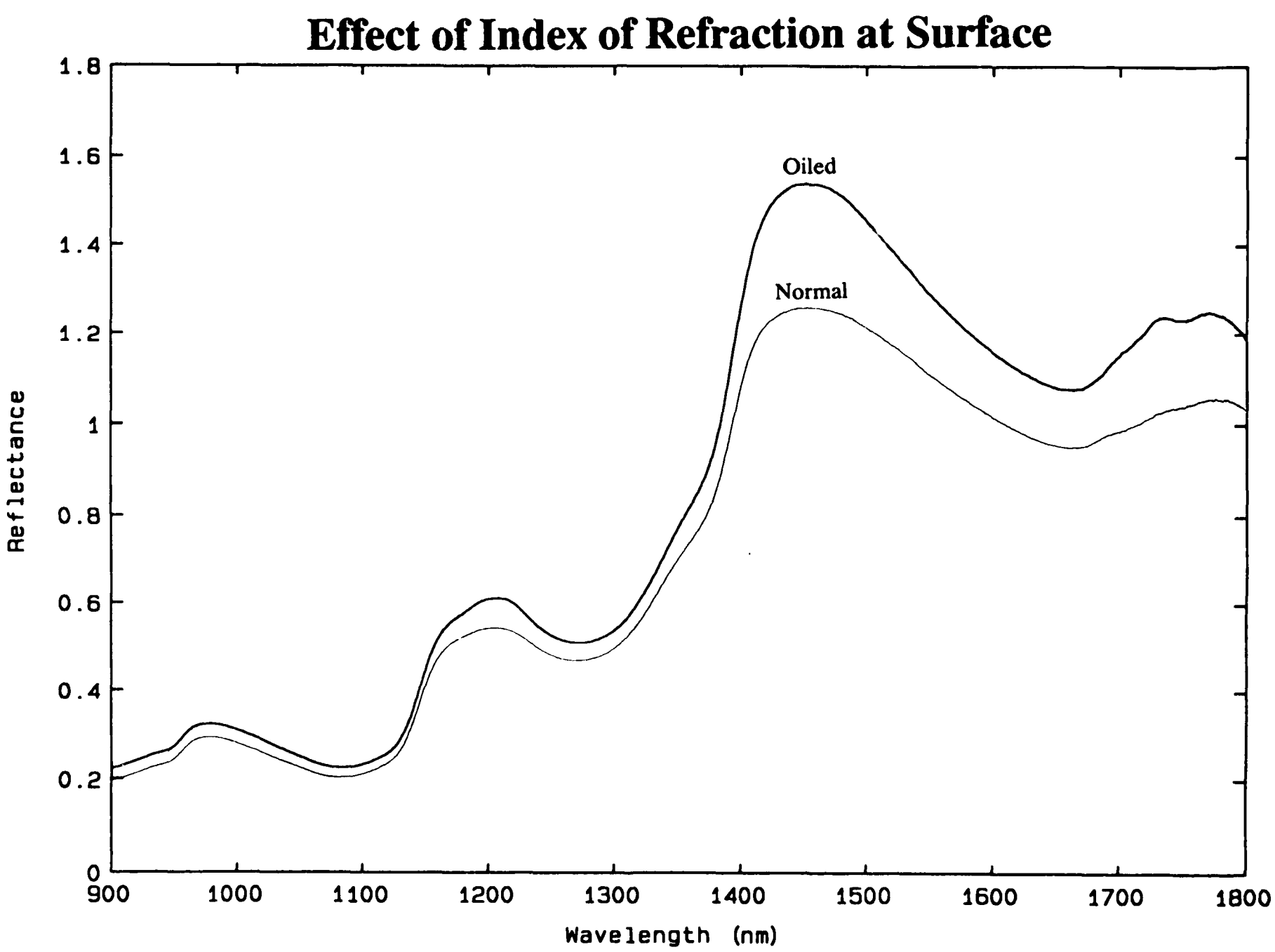
Effect of Index of Refraction at Surface
Oiled
Normal
Reflectance
Wavelength (nm)
1.8
1.6
1.4
1.2
1
0.8
0.6
0.4
0.2
0
900
1000
1100
1200
1300
1400
1500
1600
1700
1800

Figure 15

Structure of the Skin

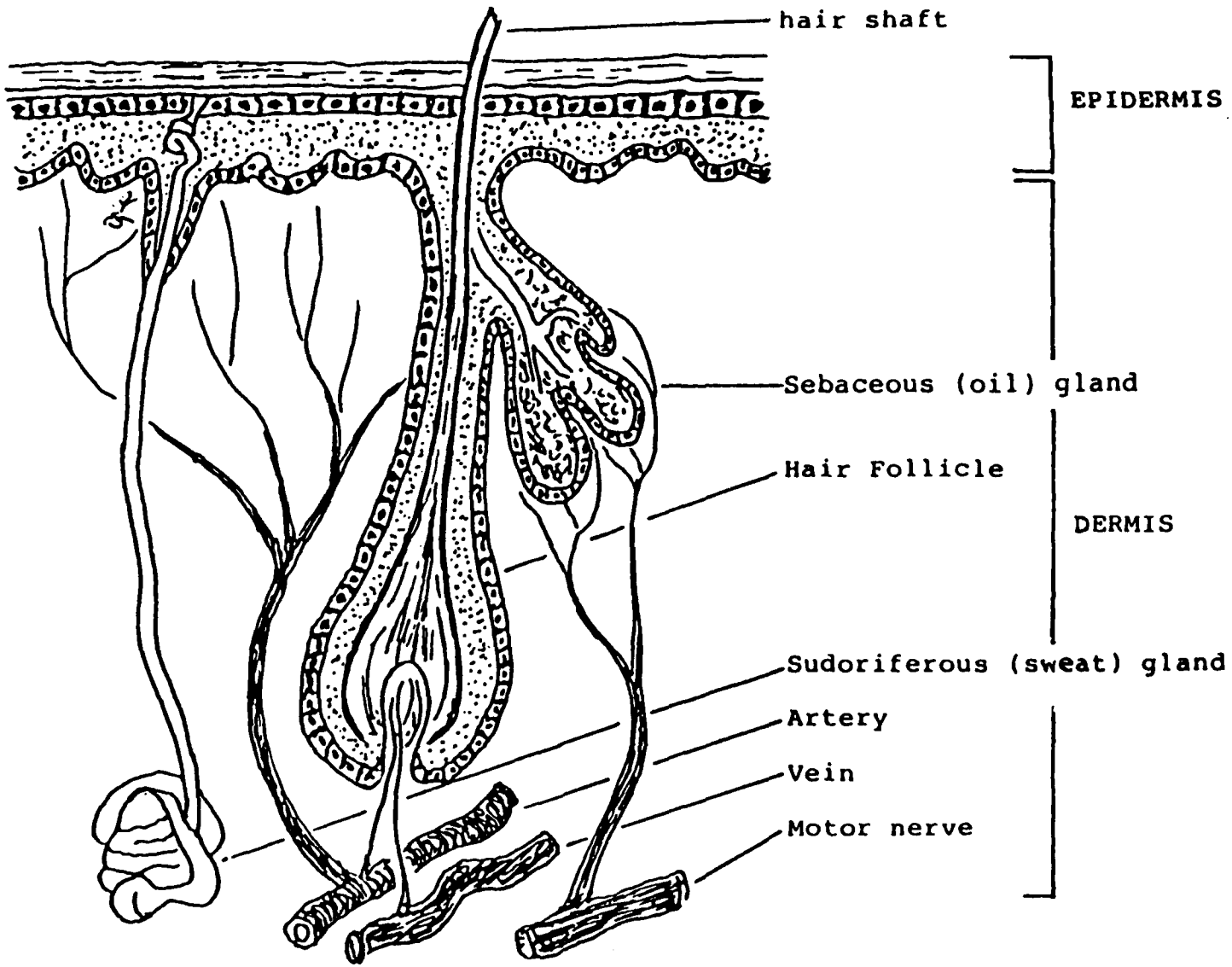

Figure 16

Denaturation of Proteins

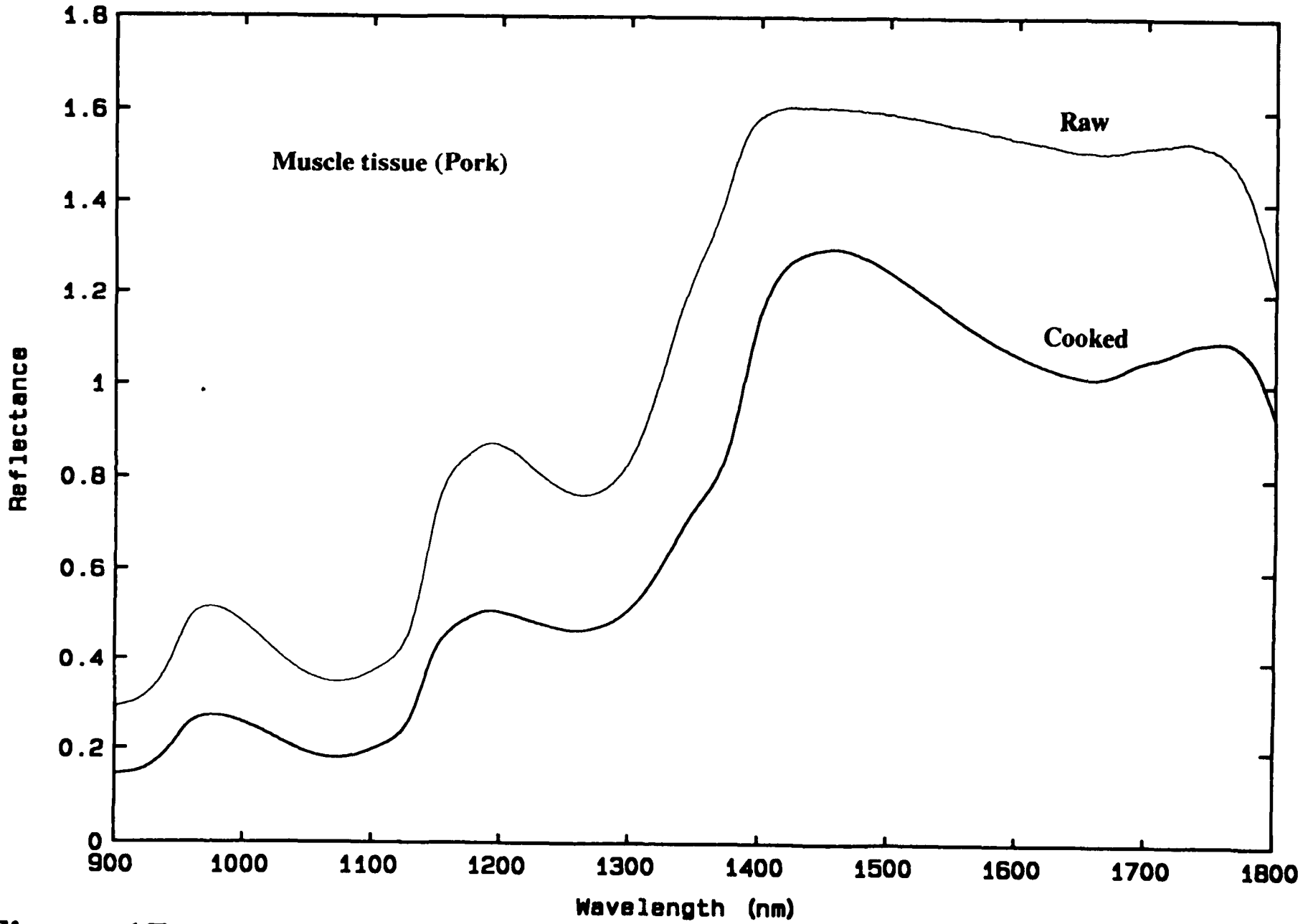

Figure 17

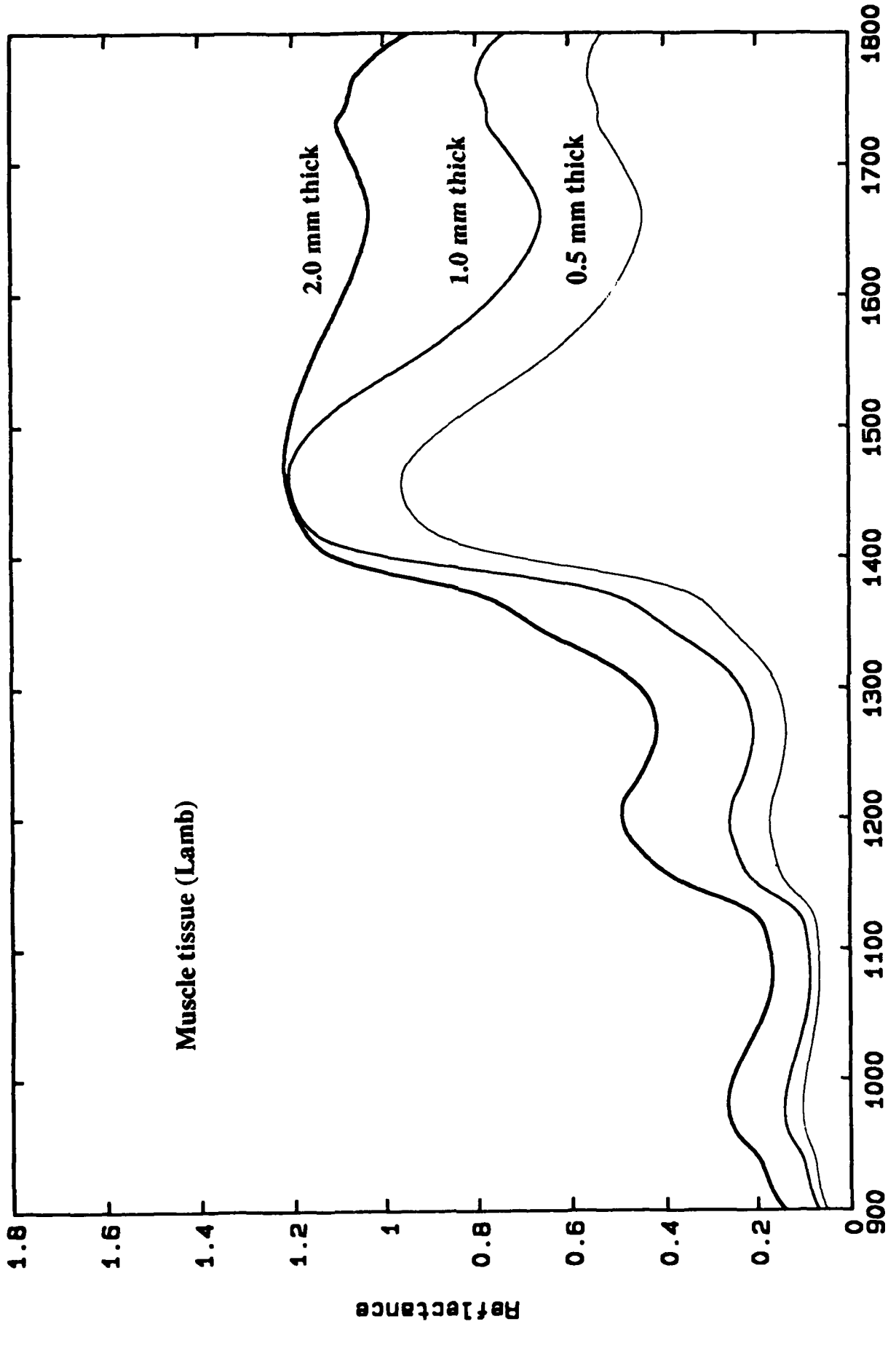
Penetration Depth
Muscle tissue (Lamb)
2.0 mm thick
1.0 mm thick
0.5 mm thick
Reflectance
Wavelength (nm)
1.8
1.6
1.4
1.2
1
0.8
0.6
0.4
0.2
0
900
1000
1100
1200
1300
1400
1500
1600
1700
1800

Figure 18

Scar Tissue

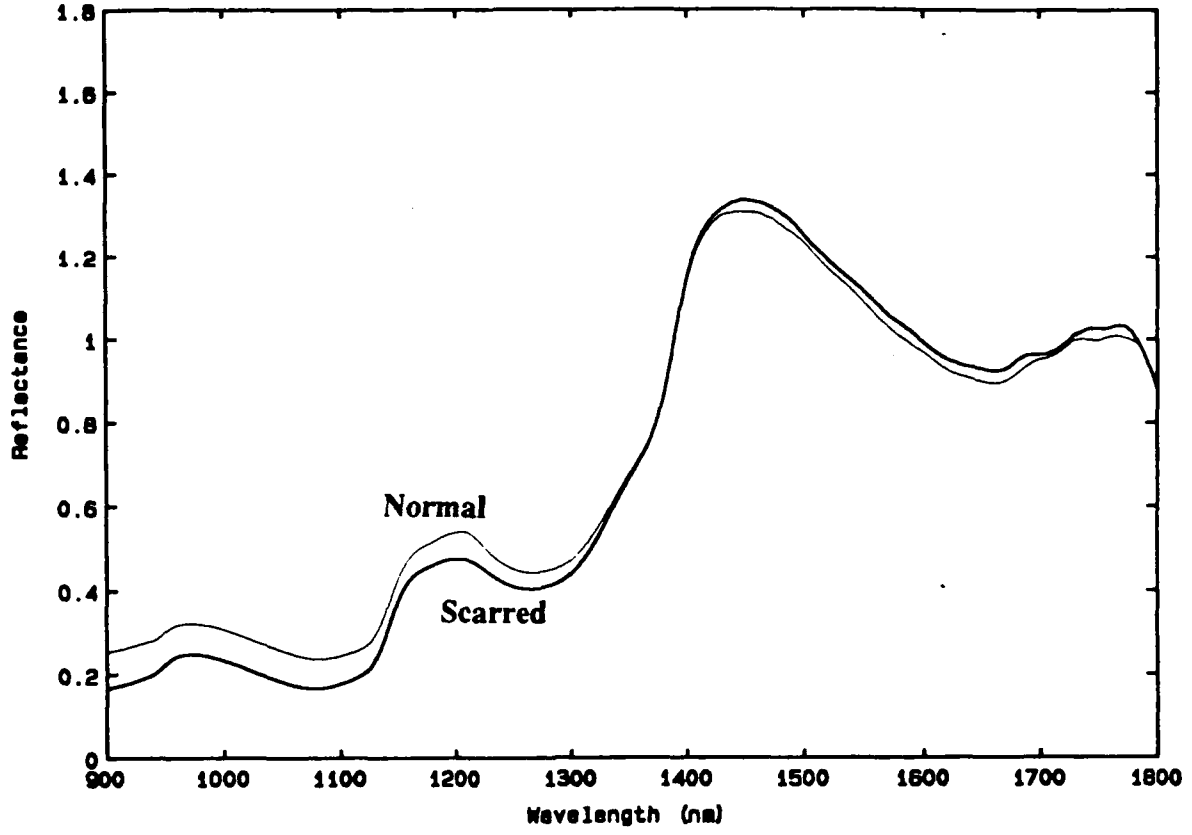

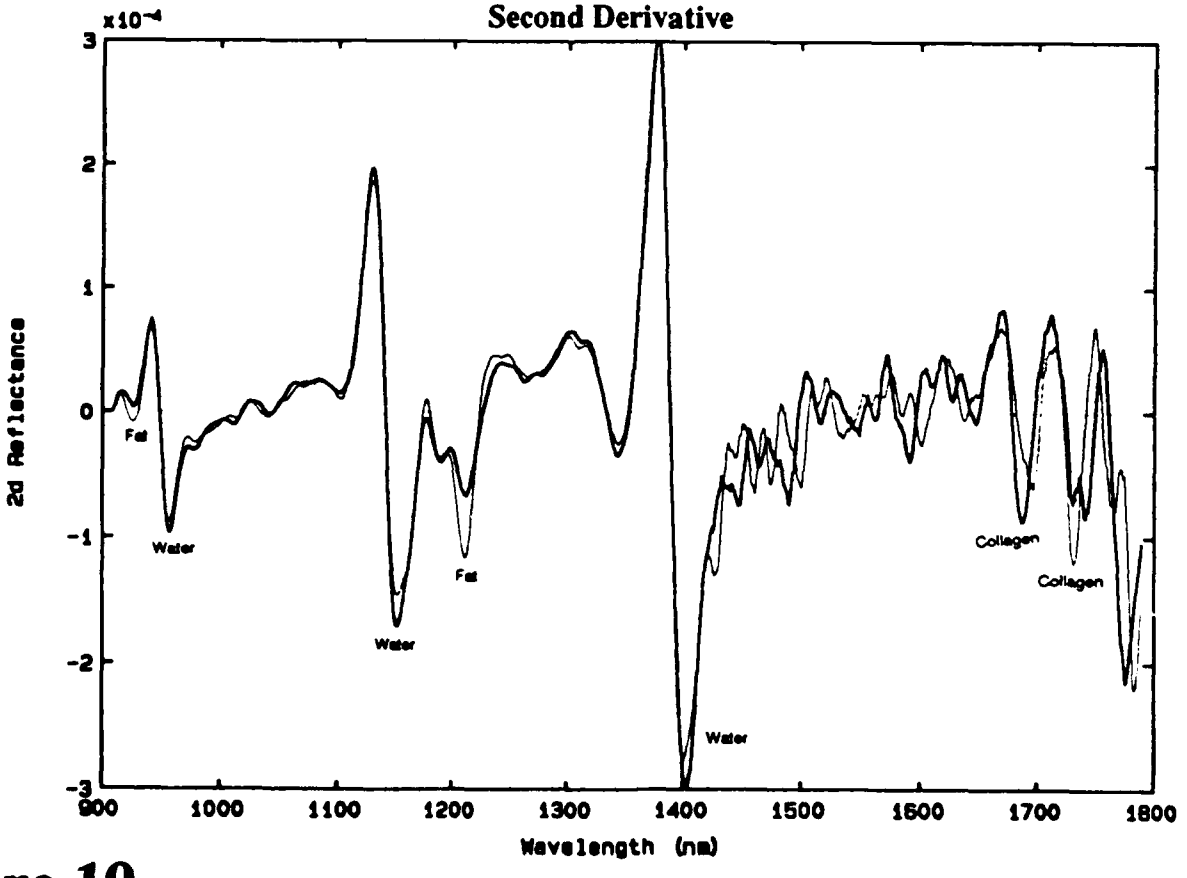

Figure 19

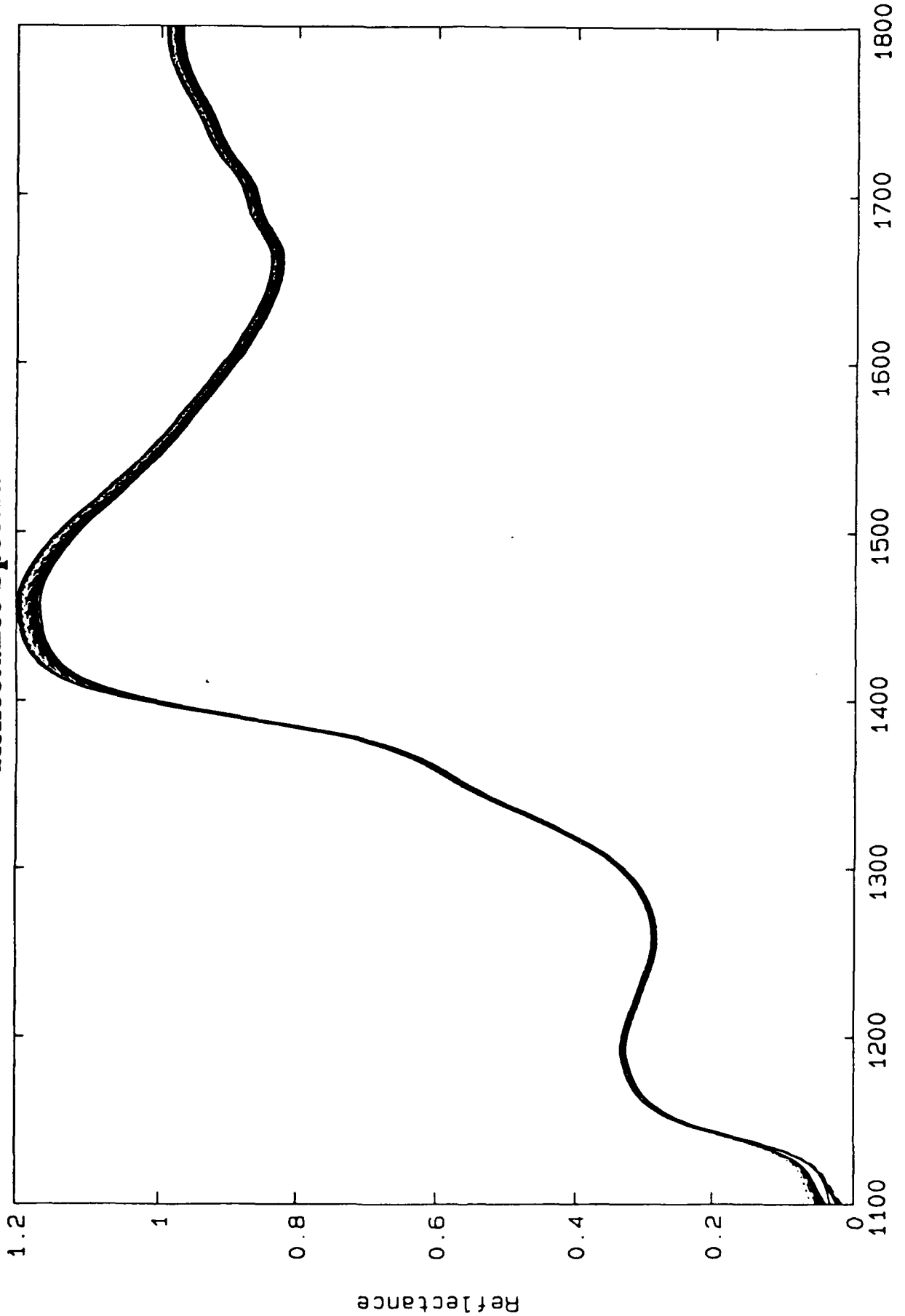
Ischemia
Reflectance Spectra
Reflectance
1.2
1
0.8
0.6
0.4
0.2
0
1100
1200
1300
1400
1500
1600
1700
1800
Wavelength (nm)

Figure 20

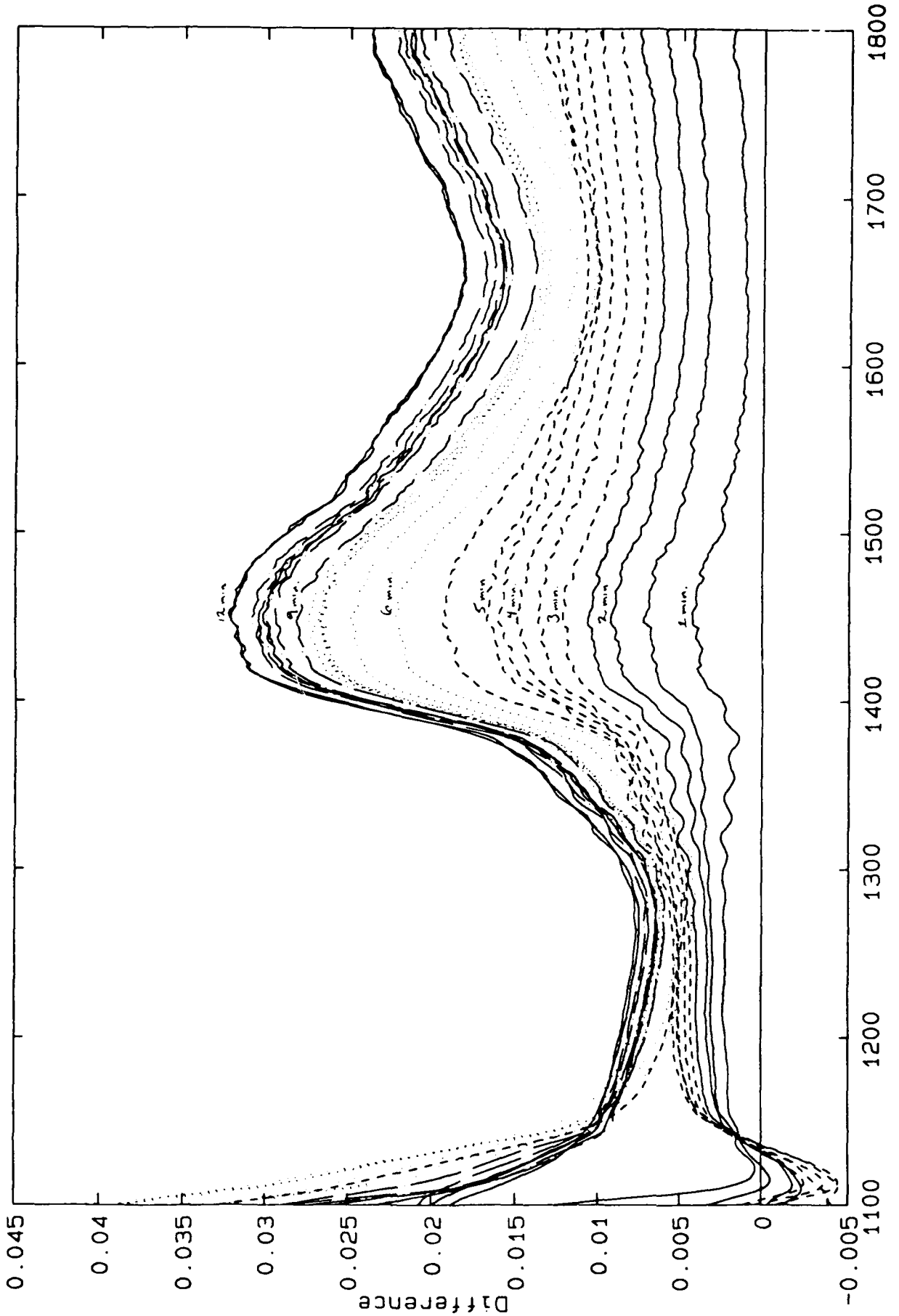
Difference (First spectrum subtracted)
Difference
Wavelength (nm)
0.045
0.04
0.035
0.03
0.025
0.02
0.015
0.01
0.005
0
-0.005
1100
1200
1300
1400
1500
1600
1700
1800
1 min.
2 min.
3 min.
4 min.
5 min.
6 min.
7 min.
12 min.

Figure 21

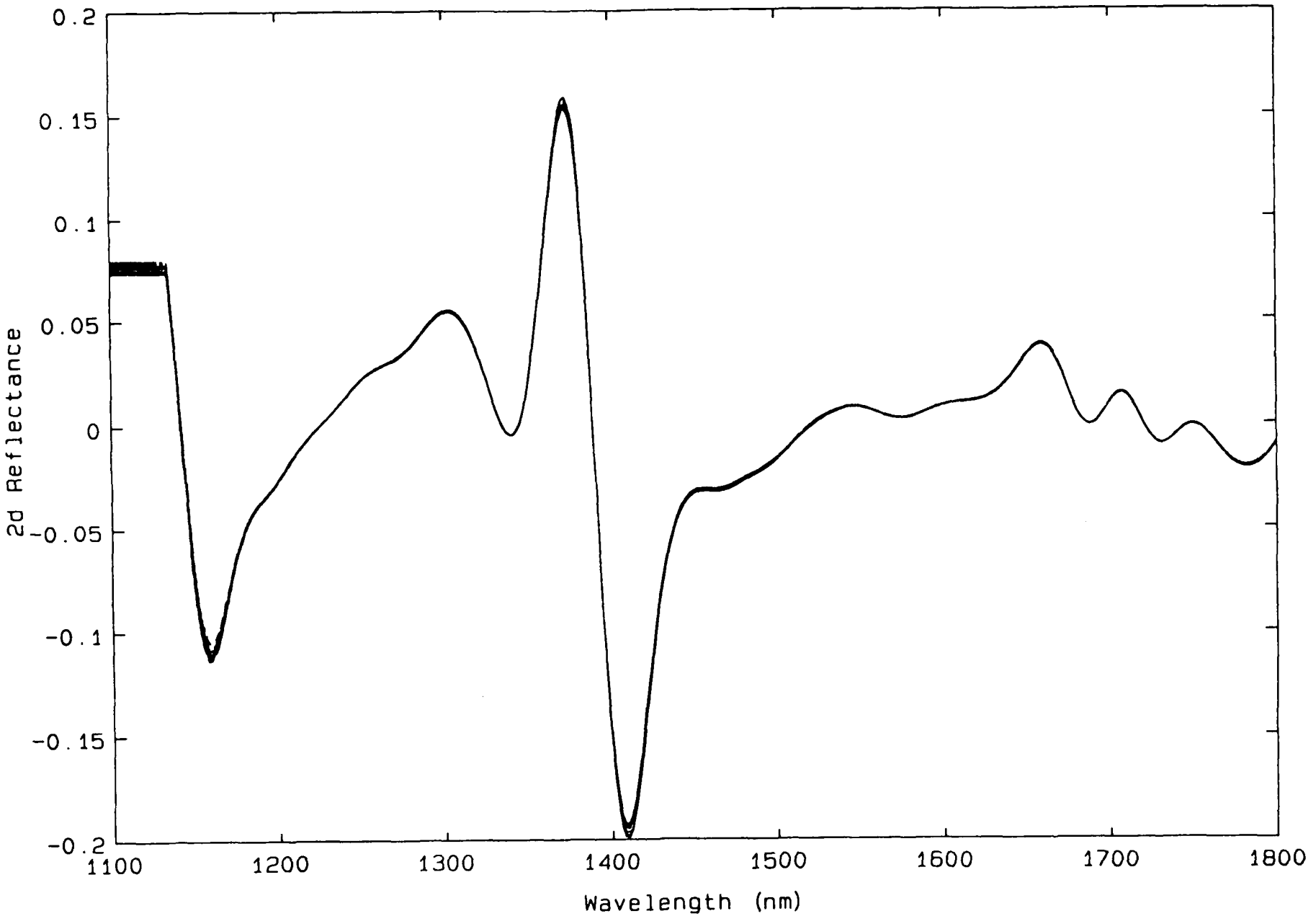
Second Derivative Spectra
0.2
0.15
0.1
0.05
0
-0.05
-0.1
-0.15
-0.2
2d Reflectance
1100
1200
1300
1400
1500
1600
1700
1800
Wavelength (nm)

Figure 22

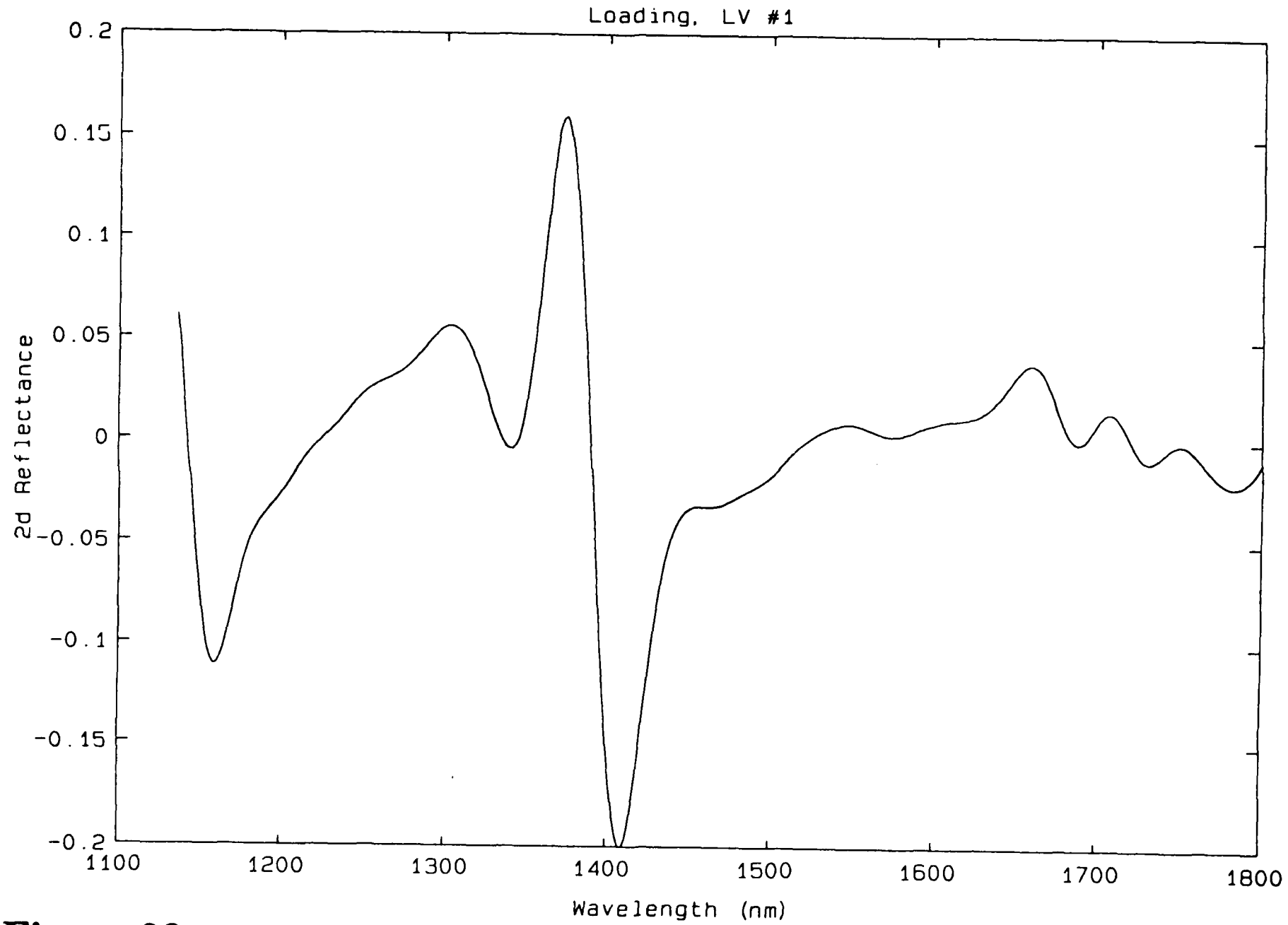
Loading, LV #1
0.2
0.15
0.1
0.05
0
-0.05
-0.1
-0.15
-0.2
2d Reflectance
1100
1200
1300
1400
1500
1600
1700
1800
Wavelength (nm)

Figure 23

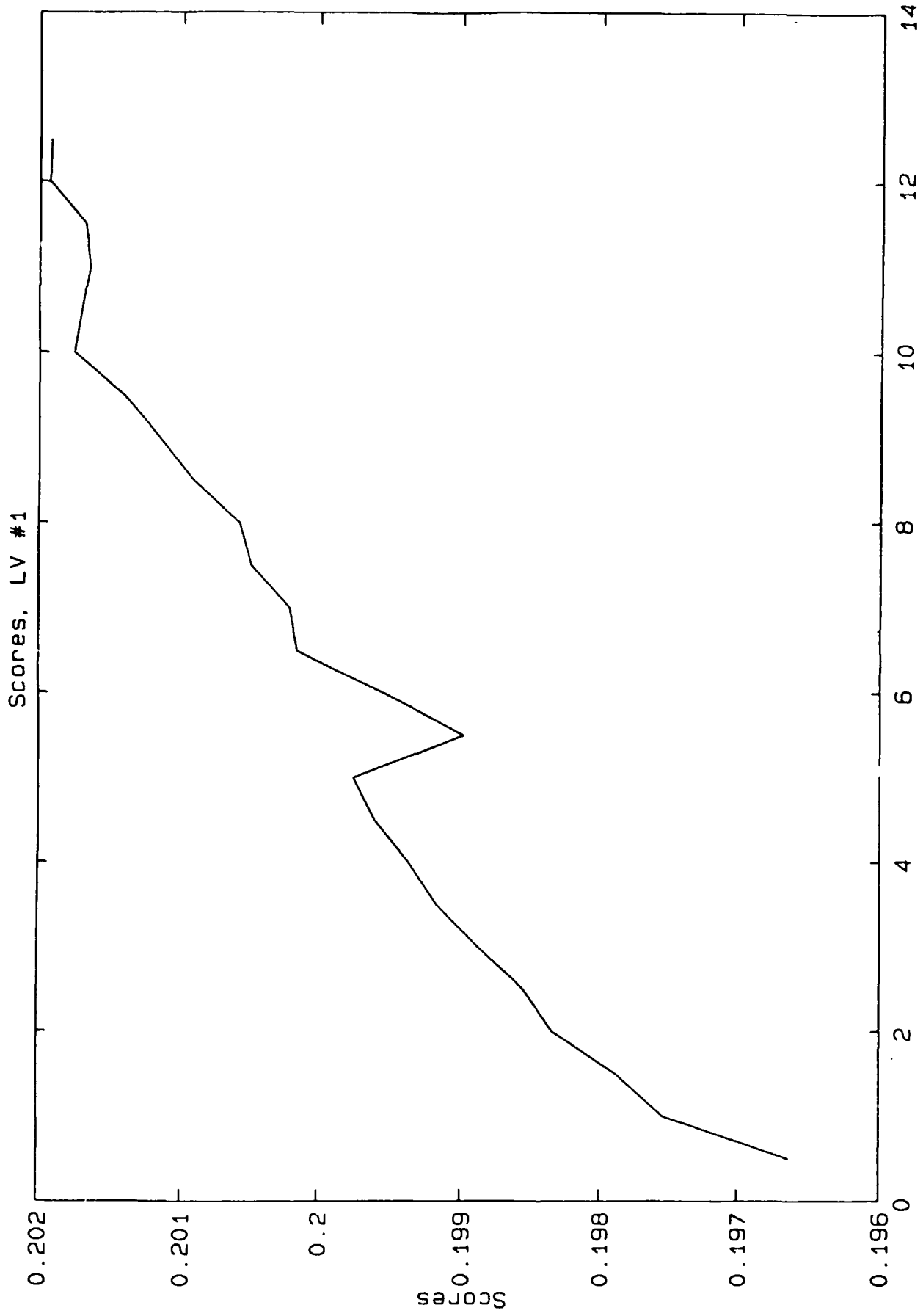
Scores, LV #1
Scores
Time (min.)
0.202
0.201
0.2
0.199
0.198
0.197
0.196
0
2
4
6
8
10
12
14

Figure 24

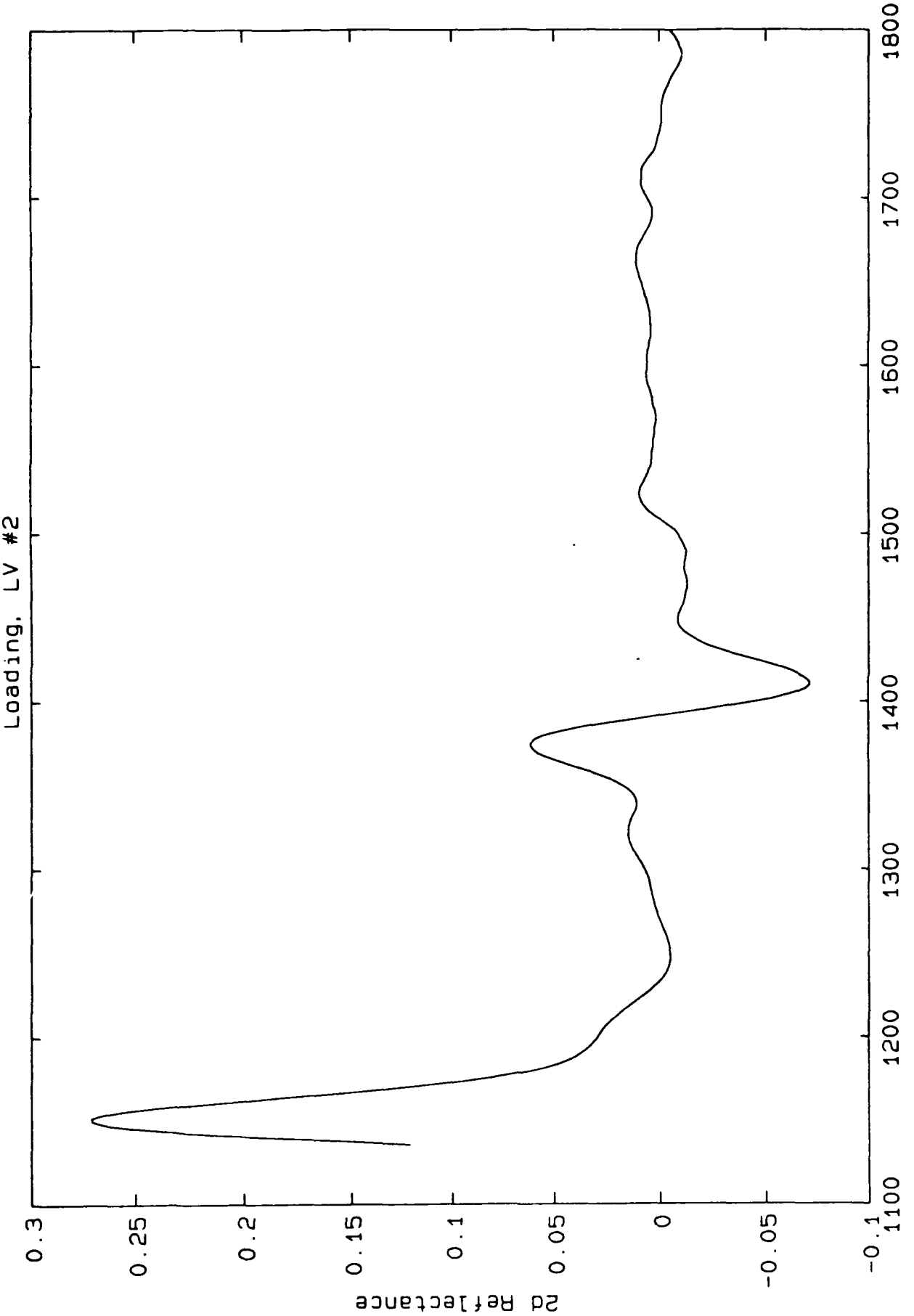
Loading, LV #2
2d Reflectance
0.3
0.25
0.2
0.15
0.1
0.05
0
-0.05
-0.1
1100
1200
1300
1400
1500
1600
1700
1800
Wavelength (nm)

Figure 25

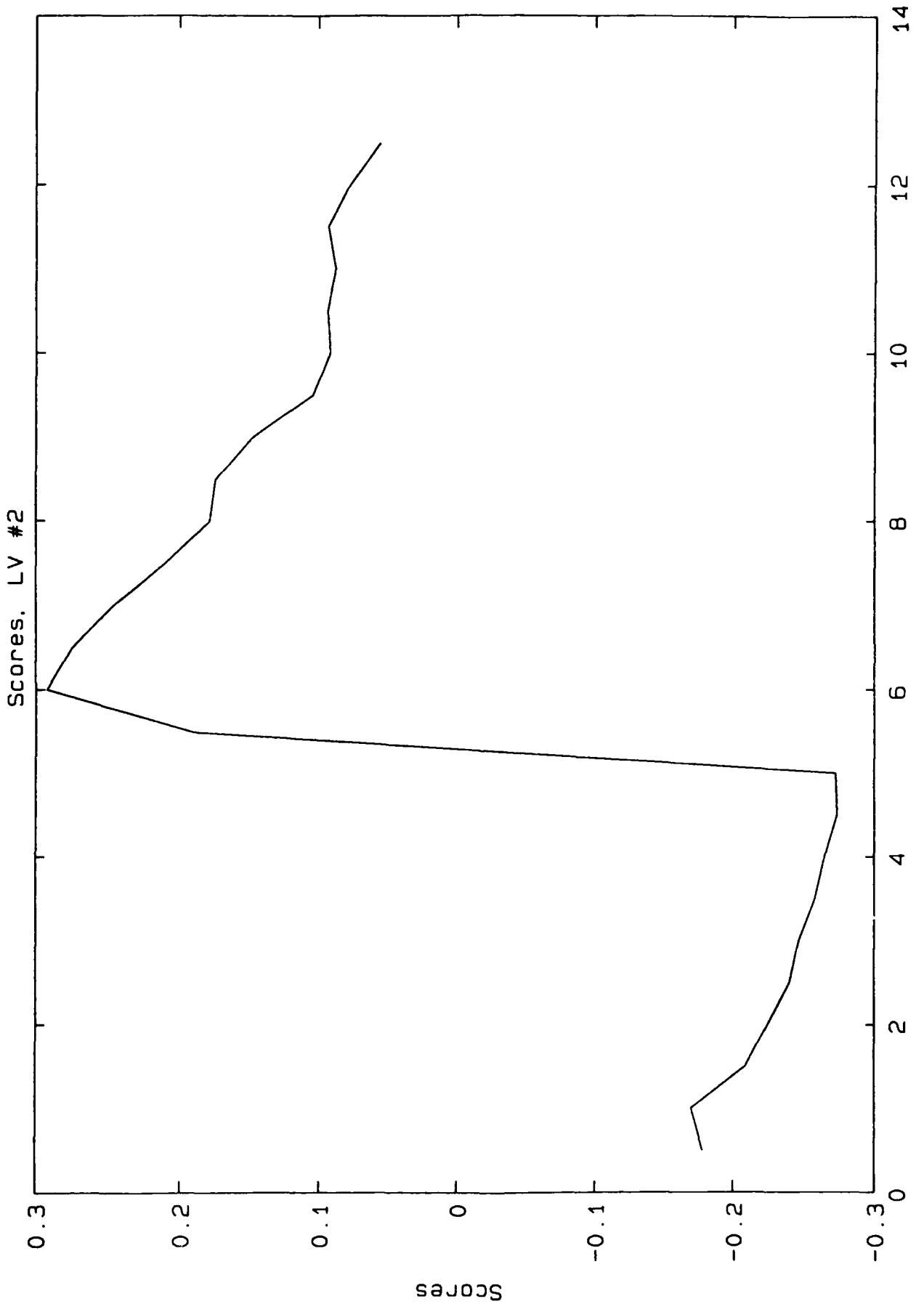

Figure 26

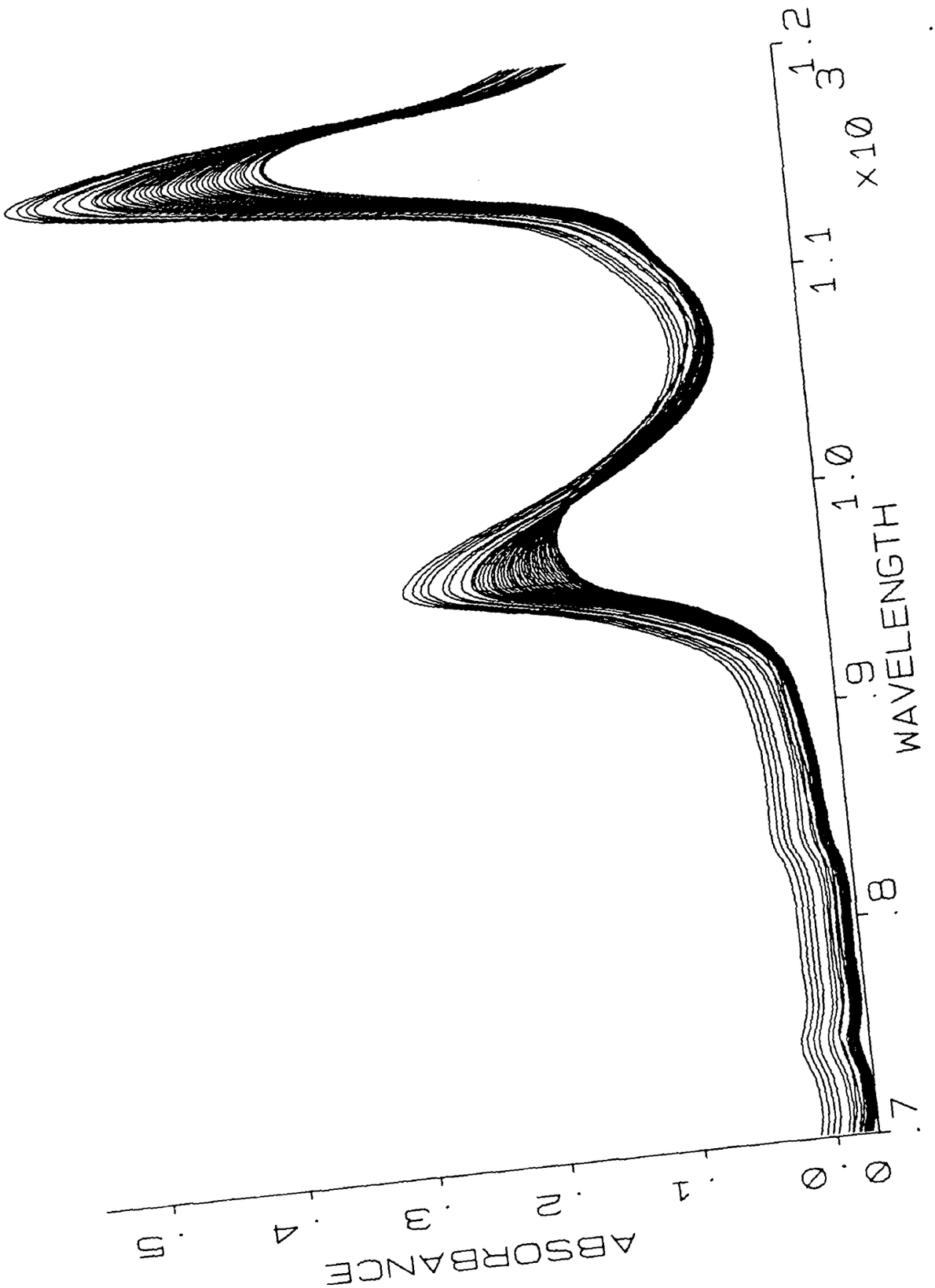

Figure 27

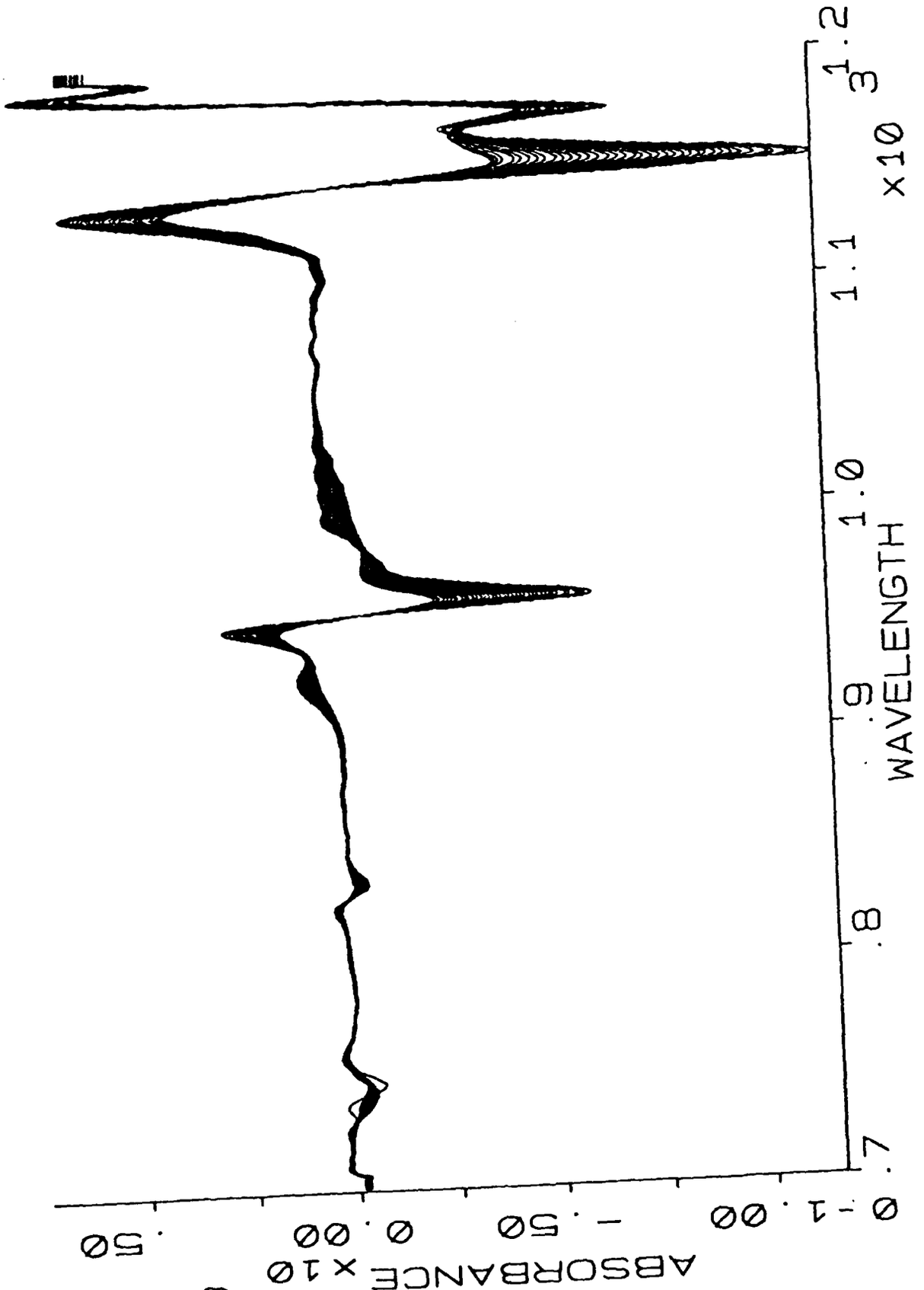

Figure 28

Figure 29

Figure 30

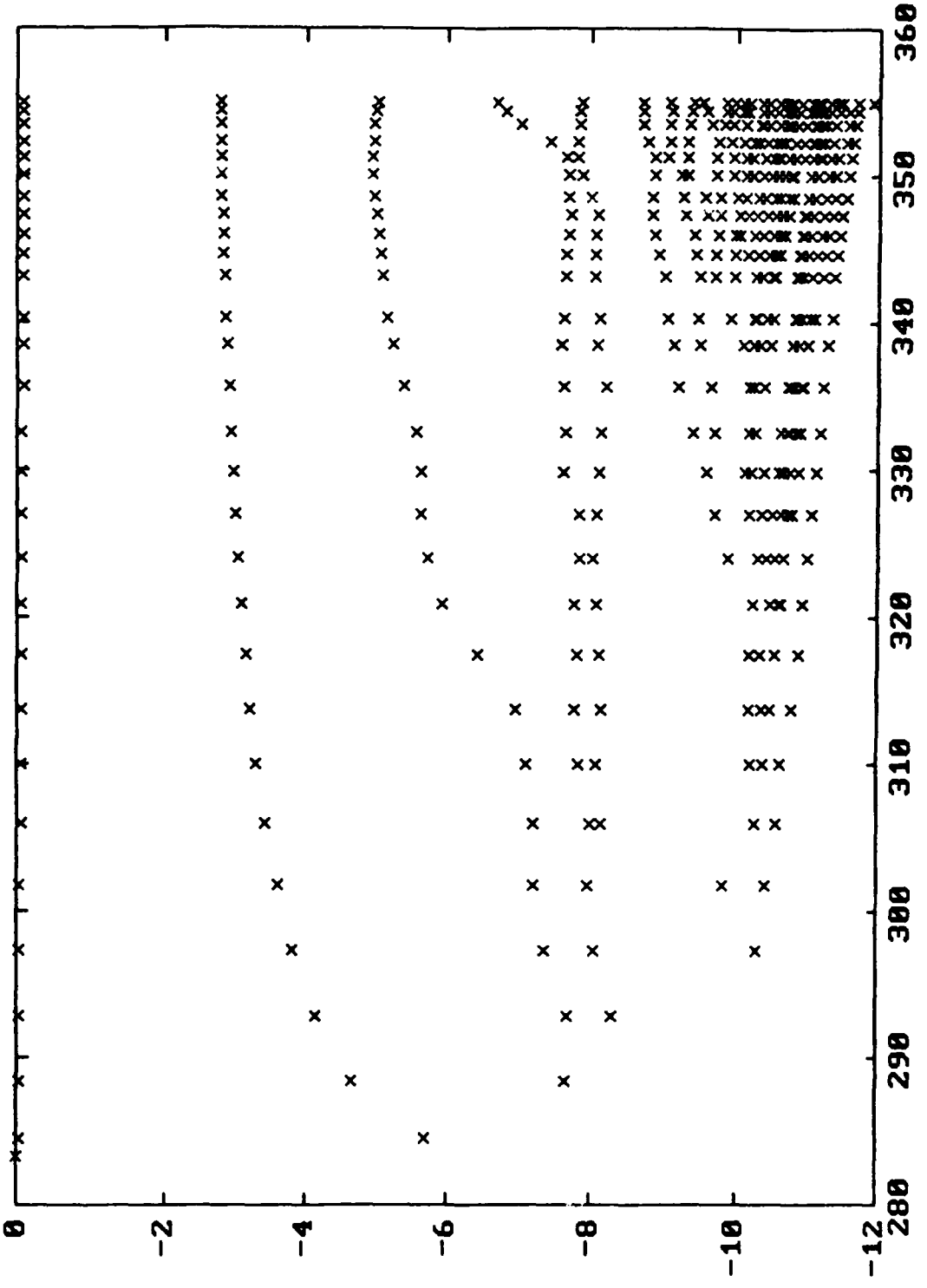

Figure 31

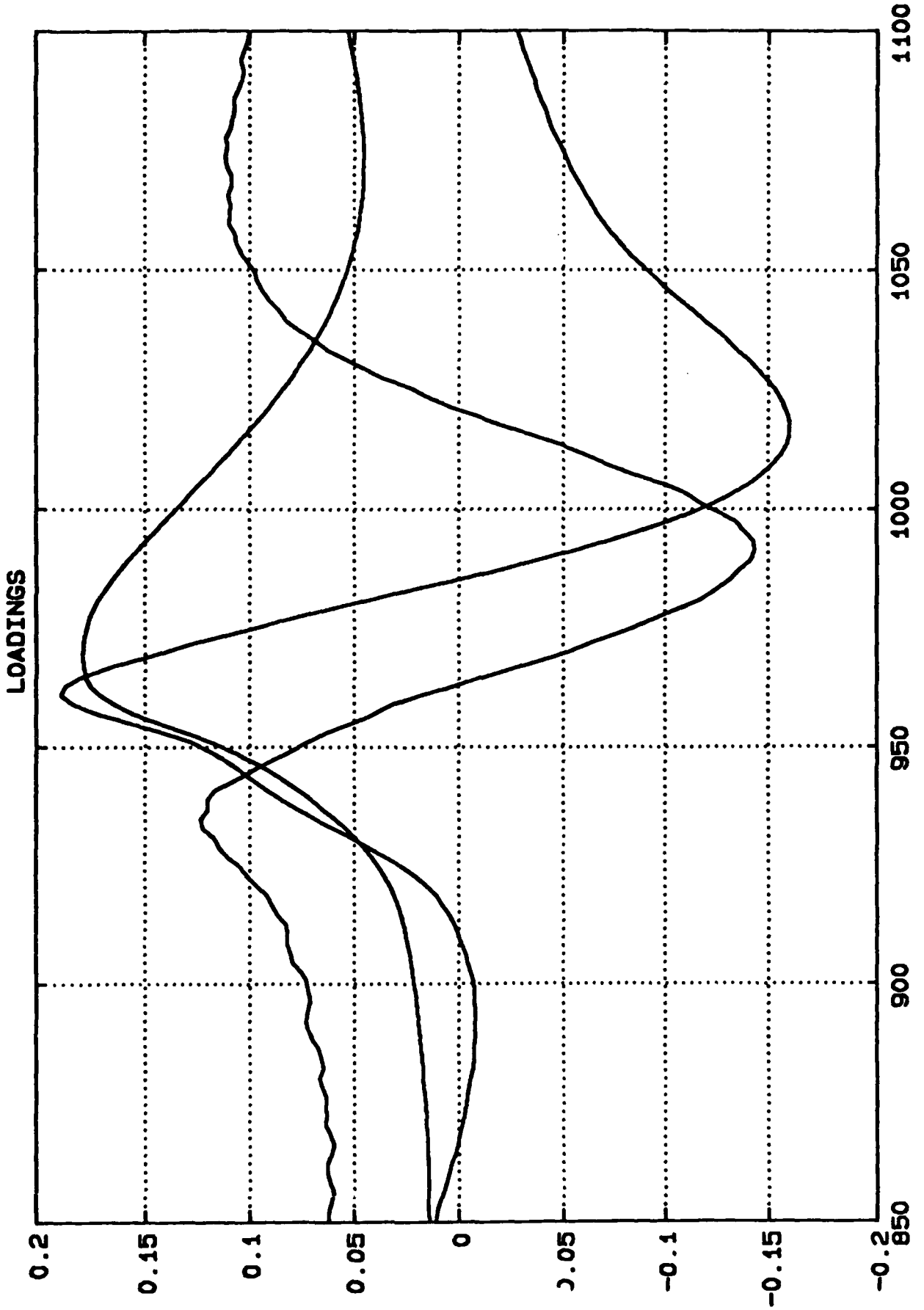
LOADINGS
0.2
0.15
0.1
0.05
0
-0.05
-0.1
-0.15
-0.2
850
900
950
1000
1050
1100
WAVELENGTH nm

Figure 32

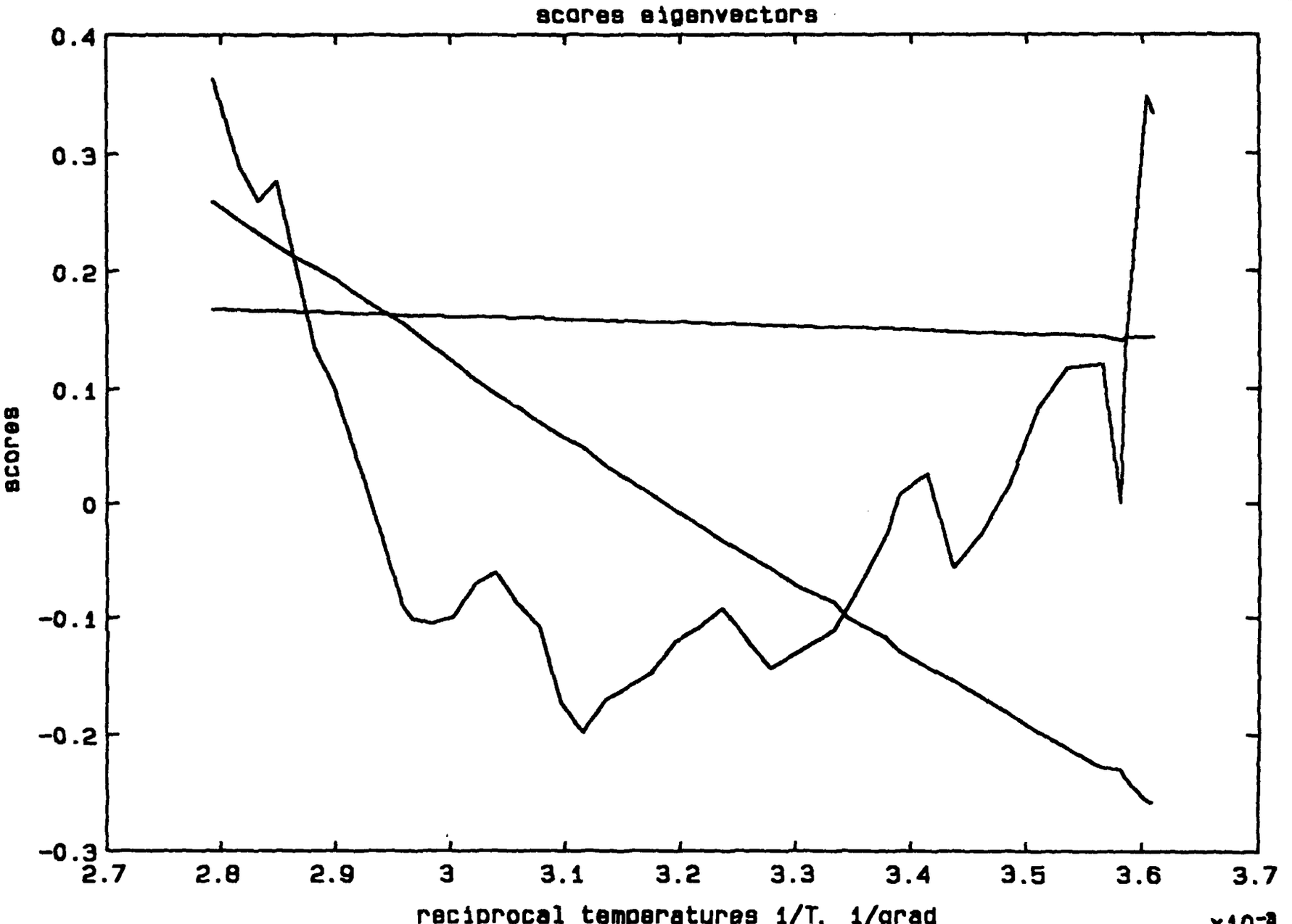
scores eigenvectors
0.4
0.3
0.2
0.1
0
-0.1
-0.2
-0.3
scores
2.7
2.8
2.9
3
3.1
3.2
3.3
3.4
3.5
3.6
3.7
reciprocal temperatures 1/T, 1/grad
x10-3

Figure 33

DISTRIBUTION LIST

4 copies	Commander Letterman Army Institute of Research (LAIR), Bldg. 1110 ATTN: SGRD-ULZ-RC Presidio of San Francisco, CA 94129-6815
1 copy	Commander US Army Medical Research and Development Command ATTN: SGRD-RMI-S Fort Detrick, Frederick, Maryland 21701-5012
2 copies	Defense Technical Information Center (DTIC) ATTN: DTIC-DDAC Cameron Station Alexandria, VA 22304-6145
1 copy	Dean School of Medicine Uniformed Services University of the Health Sciences 4301 Jones Bridge Road Bethesda, MD 20814-4799
1 copy	Commandant Academy of Health Sciences, US Army ATTN: AHS-CDM Fort Sam Houston, TX 78234-6100